«ФИЗИКА ЭЛЕМЕНТАРНЫХ ЧАСТИЦ И АТОМНОГО ЯДРА»
2000, ТОМ 31, ВЫП. 3

530.145

SEARCH FOR STANDARD HIGGS BOSON AT SUPERCOLLIDERS

N.V.Krasnikov, V.A.Matveev

INR RAS, Moscow 117312

«ФИЗИКА ЭЛЕМЕНТАРНЫХ ЧАСТИЦ И АТОМНОГО ЯДРА»
2000, ТОМ 31, ВЫП. 3

УДК 530.145

SEARCH FOR STANDARD HIGGS BOSON AT SUPERCOLLIDERS

N.V.Krasnikov, V.A.Matveev

INR RAS, Moscow 117312

We review the standard Higgs boson physics and the search for standard Higgs boson at LEP and LHC supercolliders.

Мы даем обзор вопросов, связанных с физикой стандартного бозона Хиггса и его поиском на суперколлайдерах LEP и LHC.

1. INTRODUCTION

This paper is devoted to the memory of our
teacher Nikolai Nikolaevich Bogoliubov whose
90th anniversary of the birth is celebrated
by the physical and mathematical community

The Standard Model which describes within an unprecedental scale of energies and distances the strong and electroweak interactions of elementary particles relays on a few basic principles — the renormalizability, the gauge invariance and the spontaneous breaking of the underlying gauge symmetry. The principle of the renormalizability which is considered often as something lying beyond the limits of experimental test is in fact one of the most important (if not the major) ingredients of the quantum field theory.

The requirement of renormalizabilty which content and deep meaning were uncovered in the fundamental textbook by N.N.Bogoliubov and D.V.Shirkov [1] plays the central role in the construction and classification of the field theoretic models. They split in general on two classes.

In the renormalizable models the ultraviolet divergences of the radiative corrections are under mathematically rigorous control due to the famous Bogoliubov–Parasiuk theorem [2]. These models which preserve their locality in all orders of the perturbation theory are characterised by a finite number of relevant dimensionless coupling constants whose dependence on an arbitrary dimensional normalization parameter is described by the renormalization group [1]. These so-called «running» coupling constants depending on the model may have either the asymptotic freedom behaviour at large momenta (as for non-Abelian gauge theories) or like in quantum electrodynamics with an Abelian gauge symmetry reveal the growth of the effective coupling constant in the ultraviolet region.

The second class of field theoretical models — the nonrenormalizable models have a very serious drawback which makes them useless for description of particle interactions at the present level of knowledge. First of all, the nonrenormalizable models have infinite number of divergent matrix elements which requires as a consequence an introduction of an infinite number of interaction vertices and dimensional coupling constants. What is more important the nonrenormalizable theories are nonlocal and depend on the infinite number of unknown functions [1,3]. This follows from the fact that the vertices of the nonrenormalizable models contain an arbitrary high derivatives of the field operators. Thus the predictive power of nonrenormalizable models is close to zero. An imaging world described by such a theory seems to be extremely complicated unlike what we learn from studying particle interactions and evolution of the Universe at least until the present*.

The Weinberg–Salam model [4] of the electroweak interactions belongs to the first class of the field theories. The major ingredient of this model which experimental test is the target of the world-wide search programme is the presence of the scalar multiplet with nontrivial vacuum condensate (the Higgs boson [5]). The nonzero vacuum condensate does not affect the small distance behaviour of particle interactions which allows one to solve the problem of mass generation for vector W and Z bosons without conflict with the renormalizabilty of the theory. The spontaneous breaking of the gauge symmetry in the Weinberg–Salam model is a consequence of the degeneration of the ground state in the presence of the boson condensate — in precise analogy with the theory of superfluidity [6].

In the Weinberg–Salam model a complex isodoublet scalar field is introduced through self-interactions; this acquires nonvanishing vacuum expectation value, breaking spontaneously the electroweak gauge group $SU(2)_L \otimes U(1)$ to the electromagnetic $U(1)_{EM}$ gauge group. The interactions of the gauge bosons and fermions with the background field generate the masses of these particles. One component of the scalar isodoublet Higgs field is not absorbed in the longitudinal components of the vector W and Z bosons, manifesting itself as the physical Higgs particle h**. It should be stressed that the Higgs mechanism is the only way to construct the renormalizable theory of the electroweak interactions. Therefore the discovery of the single missing ingredient of the Weinberg–Salam model — the Higgs boson will be in some sense the experimental «proof» of the renormalizability of the electroweak interactions. There are no doubts that at present the main supergoal in high energy experimental physics is the search for the Higgs boson.

*However we should not ignore the fact that the distinction between renormalizable and non-renormalizable theories is evident only within perturbation theory.

**Note that very often standard Higgs boson is denoted by capital letter H.

In this paper we present an introduction to electroweak symmetry breaking and Higgs boson physics for the Weinberg–Salam model (the Standard Model*). The current experimental status of the Higgs boson searches and implications for future experiments at the Large Hadron Collider (LHC) are discussed. We don't review the Higgs boson physics at e^+e^- linear collider [7] and at muon collider [8] because at present it is too far from reality. It should be noted that at present common belief is that the Standard Model is not the whole story and at the TeV scale new physics beyond the Standard Model exists. Namely, the most popular scenario is the low energy broken supersymmetry with the $O(1)$ TeV sparticle masses [9]. In such scenario at least two Higgs boson doublets must exist, so in addition to the standard (light) Higgs boson h there must exist scalar charged Higgs boson $H^{\pm}$, second neutral scalar Higgs boson H and axial scalar Higgs boson A. For the most interesting case when the Higgs boson h is much lighter than the additional Higgs bosons $H, H^{\pm}, A$, we have the decoupling of the heavy Higgs bosons and the interactions of the lightest Higgs boson with vector bosons and fermions coincide up to power corrections with the Standard Model interactions. Therefore even if new physics beyond the Standard Model exists at TeV region with very big probability, the physics of the lightest Higgs boson is described by the Standard Model. Note that there are several books and reviews on the Higgs boson physics [10–18]. The peculiarity of this review is that we give both theoretical aspects of the Higgs boson physics and experimental aspects related to the search for the Higgs boson at LHC.

The organization of the paper is the following. In section 2 we describe the Lagrangian of the Standard Model. In section 3 we give the main formulae for the Higgs boson decay widths. In section 4 indirect bounds on the Higgs boson mass are discussed. LEP1 and LEP2 Higgs boson mass bounds are given in section 5. The Higgs boson production mechanisms and the main formulae for the cross sections are described in section 6. In section 7 we discuss the possibilities to discover Higgs boson at upgrated TEVATRON. In section 8 we give review of the two main general purpose detectors at LHC (CMS and ATLAS). The perspectives for the search for Higgs boson at LHC are described in section 9. Section 10 contains concluding remarks.

2. THE LAGRANGIAN OF THE STANDARD MODEL

The Standard Model (SM) is the renormalizable model of strong and electroweak interactions. It has the gauge group $SU(3)_c \otimes SU(2)_L \otimes U(1)$ and the

*By the Standard Model we understand the electroweak Weinberg–Salam model plus quantum chromodynamics.

minimal Higgs structure consisting of one complex doublet of scalar particles. The spontaneous electroweak symmetry breaking $SU(3)_c \otimes SU(2)_L \otimes U(1) \to SU(3)_c \otimes U(1)_{EM}$ due to nonzero vacuum expectation value of the Higgs doublet provides the simplest realization of the Higgs mechanism [5] which generates masses for gauge $W^{\pm}$, Z bosons and masses to quarks and leptons. In this approach, the Goldstone bosons are generated by dynamics of elementary scalar fields and precisely one neutral Higgs scalar (the Higgs boson) remains in the physical spectrum. The Lagrangian of the Standard Model consists of several pieces:

$$L_{WS} = L_{YM} + L_{HYM} + L_{SH} + L_f + L_{Yuk}\,. \tag{1}$$

Here L_{YM} is the Yang–Mills Lagrangian without matter fields

$$L_{YM} = -\frac{1}{4}F^i_{\mu\nu}(W)F^{\mu\nu}_i(W) - \frac{1}{4}F^{\mu\nu}(W^0)F_{\mu\nu}(W^0) - \frac{1}{4}F^a_{\mu\nu}(G)F^{\mu\nu}_a(G)\,, \tag{2}$$

where $F^i_{\mu\nu}(W)$, $F^a_{\mu\nu}(G)$, $F_{\mu\nu}(W^0)$ are given by

$$F^i_{\mu\nu}(W) = \partial_\mu W^i_\nu - \partial_\nu W^i_\mu + g_2\epsilon^{ijk}W^j_\mu W^k_\nu\,, \tag{3}$$

$$F_{\mu\nu}(W^0) = \partial_\mu W^0_\nu - \partial_\nu W^0_\mu\,, \tag{4}$$

$$F^a_{\mu\nu}(G) = \partial_\mu G^a_\nu - \partial_\nu G^a_\mu + g_s f^{abc}G^b_\mu G^c_\nu\,, \tag{5}$$

where W^i_μ, W^0_μ are the $SU(2)_L \otimes U(1)$ gauge fields, G^a_μ are the gluon fields and ϵ^{ijk}, f^{abc} are the structure constants of the $SU(2)_L$ and $SU(3)_c$ gauge groups. The Lagrangian L_{HYM} describes the Higgs doublet interaction with $SU(2)_L \otimes U(1)$ gauge fields

$$L_{HYM} = (D_{L\mu}H)^+(D^\mu_L H)\,, \tag{6}$$

where covariant derivatives are given by

$$D_{L\mu} = \partial_\mu - ig_1\frac{Y}{2}W^0_\mu - ig_2\frac{\sigma^i}{2}W^i_\mu\,, \tag{7}$$

$$D_{R\mu} = \partial_\mu - ig_1\frac{Y}{2}W^0_\mu\,, \tag{8}$$

$$D^q_{L\mu} = \partial_\mu - ig_1\frac{Y}{2}W^0_\mu - ig_2\frac{\sigma^i}{2}W^i_\mu - ig_3t^aG^a_\mu\,, \tag{9}$$

$$D^q_{R\mu} = \partial_\mu - ig_1\frac{Y}{2}W^0_\mu - ig_3 t^a G^a_\mu\,. \tag{10}$$

Here g_1 is the $U(1)$ gauge coupling constant, g_2 and g_3 are the $SU(2)_L$ and $SU(3)_c$ gauge coupling constants, Y is the hypercharge determined by the relation $Q = \frac{\sigma_3}{2} + \frac{Y}{2}$, σ^i are the Pauli matrices, t^a are $SU(3)$ matrices in the fundamental representation, $H = \begin{pmatrix} H_1 \\ H_2 \end{pmatrix}$ is the Higgs $SU(2)_L$ doublet with $Y = 1$. The Lagrangian L_{SH} describing Higgs doublet self-interaction has the form

$$L_{SH} = -V_0(H) = M^2 H^+ H - \frac{\lambda}{2}(H^+ H)^2\,, \tag{11}$$

where $H^+H = \sum_i H^*_i H_i$ and λ is the Higgs self-coupling constant. The Lagrangian L_f describes the interaction of fermions with gauge fields. Fermions constitute only doublets and singlets in $SU(2)_L \otimes U(1)$

$$R_1 = e_R,\ R_2 = \mu_R,\ R_3 = \tau_R\,, \tag{12}$$

$$L_1 = \begin{pmatrix}\nu \\ e\end{pmatrix}_L, L_2 = \begin{pmatrix}\nu' \\ \mu\end{pmatrix}_L, L_3 = \begin{pmatrix}\nu'' \\ \tau\end{pmatrix}_L, \tag{13}$$

$$R_{qIu} = (q_{Iu})_R,\ \ (q_{1u} = u,\ q_{2u} = c,\ q_{3u} = t)\,, \tag{14}$$

$$R_{qid} = (q_{id})_R,\ \ (q_{1d} = d,\ q_{2d} = s,\ q_{3d} = b)\,, \tag{15}$$

$$L_{qI} = \begin{pmatrix} q_{Iu} \\ V_{Ii}q_{id}\end{pmatrix}_L, \tag{16}$$

where L and R denote left- and right-handed components of the spinors respectively,

$$\psi_{R,L} = \frac{1 \pm \gamma_5}{2}\psi \tag{17}$$

and V_{Ii} is the Kobayashi–Maskawa matrix. The neutrinos are assumed to be left-handed and massless. The Lagrangian L_f describes the interaction of fermions with gauge fields and it has the form

$$L_f = \sum_{k=1}^{3}[i\bar{L}_k\hat{D}_L L_k + i\bar{R}_k\hat{D}_R R_k + i\bar{L}_{qk}\hat{D}^q_L L_{qk} +$$

$$+ i\bar{R}_{qku}\hat{D}^q_R R_{qku} + i\bar{R}_{qkd}\hat{D}^q_R R_{qkd}]\,, \tag{18}$$

where $\hat{D}_L = \gamma^\mu D_{L\mu}$, $\hat{D}_R = \gamma^\mu D_{R\mu}$, $\hat{D}^q_L = \gamma^\mu D^q_{L\mu}$, $\hat{D}^q_R = \gamma^\mu D^q_{R\mu}$. The Lagrangian L_{Yuk} generates fermion mass terms. Supposing the neutrinos to be

massless, the Yukawa interaction of the fermions with Higgs doublet has the form

$$L_{Yuk} = -\sum_{k=1}^{3}[h_{lk}\bar{L}_k H R_k + h_{dk}\bar{L}^{'}_{qk} H R_{dk} + h_{uk}\bar{L}^{'}_{qk}(i\sigma^2 H^*)R_{uk}] + h.c.\,, \tag{19}$$

$$L^{'}_{qI} = \begin{pmatrix} q_{Iu} \\ q_{Id} \end{pmatrix}.$$

The potential term $V_0(H) = -M^2 H^+ H + \frac{\lambda}{2}(H^+ H)^2$ for $M^2 > 0$ gives rise to the spontaneous symmetry breaking. The doublet H acquires the nonzero vacuum expectation value

$$< H >= \begin{pmatrix} 0 \\ \frac{v}{\sqrt{2}} \end{pmatrix}, \tag{20}$$

where $v = 246$ GeV. In the unitary gauge unphysical Goldstone massless fields are absent and the Higgs doublet scalar field depends on the single physical scalar field $h(x)$ (Higgs boson field):

$$H(x) = \begin{pmatrix} 0 \\ \frac{v}{\sqrt{2}} + \frac{h(x)}{\sqrt{2}} \end{pmatrix}. \tag{21}$$

Due to spontaneous gauge symmetry breaking gauge fields except gluon and photon fields acquire masses. Diagonalization of mass matrix gives

$$W^{\pm}_{\mu} = \frac{1}{\sqrt{2}}(W^1_{\mu} \mp W^2_{\mu}),\ M_W = \frac{1}{2} g_2 v\,, \tag{22}$$

$$Z_{\mu} = \frac{1}{\sqrt{g_2^2 + g_1^2}}(g_2 W^3_{\mu} - g_1 W^0_{\mu}),\ M_Z = \frac{1}{2}\sqrt{g_2^2 + g_1^2}\, v\,, \tag{23}$$

$$A_{\mu} = \frac{1}{\sqrt{q_2^2 + g_1^2}}(g_1 W^3_{\mu} + g_2 W^0_{\mu}),\ M_A = 0\,, \tag{24}$$

where $W^{\pm}_{\mu}$, Z_{μ} are charged and neutral electroweak boson fields, A_{μ} is photon field. It is convenient to introduce rotation angle θ_W between (W^3, W^0) and (Z, A) which is called Weinberg angle

$$\sin\theta_W \equiv \frac{g_1}{\sqrt{g_1^2 + g_2^2}}\,. \tag{25}$$

Experimentally $\sin^2\theta_W \approx 0.23$ [19]. The formula for the electric charge e has the form

$$e = \frac{g_2 g_1}{\sqrt{g_2^2 + g_1^2}}\,. \tag{26}$$

At the tree level the Higgs boson mass is determined by the formula

$$m_h = \sqrt{2}M = \sqrt{\lambda}v\,. \tag{27}$$

The Lagrangian L_{HYM} describes the interaction of the Higgs boson field with vector W- and Z-bosons. In the unitary gauge it reads

$$L_{HYM} = \frac{1}{2}\partial^\mu h \partial_\mu h + M_W^2(1+\frac{h}{v})^2 W_\mu^+ W^\mu + \frac{1}{2}M_Z^2(1+\frac{h}{v})^2 Z^\mu Z_\mu\,. \tag{28}$$

The Lagrangian L_{Yuk} is responsible for the fermion masses generation. In the unitary gauge it can be written in the form

$$L_{Yuk} = -\sum_i m_{\psi_i}(1+\frac{h}{v})\bar{\psi}_i\psi_i\,, \tag{29}$$

where ψ_i are the fermion(quark and lepton) fields.

3. INDIRECT HIGGS BOSON MASS BOUNDS

3.1. Tree-Level Unitarity. The Higgs boson has been introduced as a fundamental particle to render 2 - 2 scattering amplitudes (see Fig. 1) involving longitudinally polarized W bosons compatible with unitarity. In general particles must decouple from low energy spectrum if their mass grows indefinitely. Therefore the Higgs boson mass must be bounded to restore unitarity in the perturbation theory. The asymptotic tree-level formula for the elastic $W_L W_L$ S-wave-scattering amplitude reads [20, 21]

$$A^{J=0}(W_L W_L \to W_L W_L) \approx -\frac{G_F m_h^2}{4\sqrt{2}\pi}. \tag{30}$$

Partial wave unitarity implies that

$$|A^J|^2 \le |Im(A^J)|, \tag{31}$$

$$(Re(A^J))^2 \le |Im(A^J)(1-|Im(A^J)|)|. \tag{32}$$

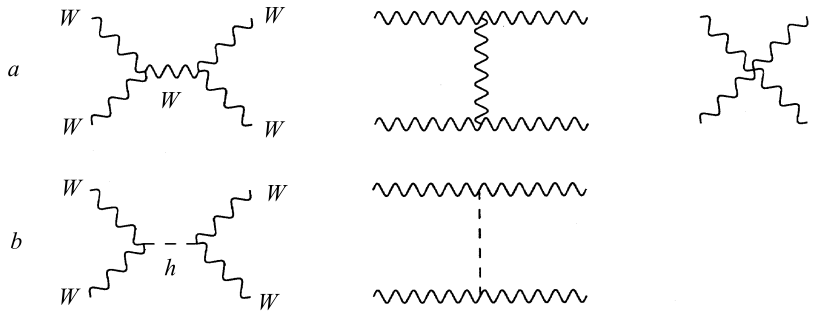

Fig. 1. Tree-level diagrams of elastic WW scattering: (*a*) pure gauge-boson dynamics, and (*b*) Higgs boson exchange

As a consequence we find that

$$|Re(A^J)| \leq \frac{1}{2}. \tag{33}$$

Hence [20, 21],

$$m_h^2 \leq \frac{2\pi\sqrt{2}}{G_F} \approx (850 \text{ GeV})^2. \tag{34}$$

The most stringent bound is obtained by performing a full coupled channel analysis for the scattering of longitudinal gauge bosons into $W_L^+W_L^-, Z_LZ_L, Z_Lh$ and hh. The largest eigenvalue of the amplitude matrix gives the most restrictive bound

$$m_h^2 \leq \frac{4\pi\sqrt{2}}{3G_F} \approx (700 \text{ GeV})^2. \tag{35}$$

However it should be noted that if $m_h \geq 700$ GeV it means simply that perturbation theory is no longer reliable and in principle an account of higher order corrections can restore unitarity. Lattice estimates give similar bound [22] $m_h \leq 700$ GeV on the Higgs boson mass.

3.2. Vacuum Stability Bound. It is possible also to derive bounds on the Higgs boson mass from the requirement of the absence of the Landau pole singularity for the effective Higgs self-coupling constant [23] and from the vacuum stability requirement [24].

The idea of the derivation of the bound resulting from the requirement of the absence of Landau pole singularities is the following [23]. Suppose the Standard Model is valid up to the scale Λ. We require that the effective Higgs self-coupling constant does not have Landau pole singularities up to the energies Λ.

From this requirement we find an upper bound on the low energy Higgs self-coupling constant $\bar{\lambda}(m_t)$ which determines the Higgs boson mass. Namely, the renormalization group equations for the effective coupling constants in neglection of all Yukawa coupling constants except top-quark Yukawa coupling constant in one-loop approximation read

$$\frac{d\bar{g}_3}{dt} = -7\bar{g}_3^3\,, \tag{36}$$

$$\frac{d\bar{g}_2}{dt} = -(\frac{19}{6})\bar{g}_2^3\,, \tag{37}$$

$$\frac{d\bar{g}_1}{dt} = (\frac{41}{6})\bar{g}_1^3\,, \tag{38}$$

$$\frac{d\bar{h}_t}{dt} = (\frac{9\bar{h}_t^2}{2} - 8\bar{g}_3^2 - \frac{9\bar{g}_2^2}{4} - \frac{17\bar{g}_1^2}{12})\bar{h}_t\,, \tag{39}$$

$$\frac{d\bar{\lambda}}{dt} = 12(\bar{\lambda}^2 + (\bar{h}_t^2 - \frac{\bar{g}_1^2}{4} - \frac{3\bar{g}_2^2}{4})\lambda - \bar{h}_t^4 + \frac{\bar{g}_1^4}{16} + \frac{\bar{g}_1^2\bar{g}_2^2}{8} + \frac{3\bar{g}_2^4}{16})\,, \tag{40}$$

$$t = (\frac{1}{16\pi^2})\ln(\mu/m_Z)\,. \tag{41}$$

Here $\bar{g}_3$, $\bar{g}_2$ and $\bar{g}_1$ are the $SU(3)_c$, $SU(2)_L$ and $U(1)$ effective gauge couplings, respectively, and $\bar{h}_t$ is the effective top-quark Yukawa coupling constant. In our concrete estimates we took $m_t^{\rm pole} = 175$ GeV, $\bar{\alpha}_3(m_Z) = 0.118$, $\bar{\alpha}_{em}^{-1}(m_Z) = 127.9$, $\sin^2\theta_W(m_Z) = 0.2337$, $\alpha_i \equiv \frac{g_i^2}{4\pi}$. From the requirement of the absence of Landau pole singularity for the Higgs self-coupling constant $\bar{\lambda}$ for the scales up to $\Lambda = (10^3; 10^4; 10^6; 10^8; 10^{10}; 10^{12}; 10^{14})$ GeV (to be precise we require that at the scale Λ the Higgs self-coupling constant is $\frac{\bar{\lambda}^2(\Lambda)}{4\pi} \leq 1$) we have found the upper bound on the Higgs boson mass $m_h \leq (400; 300; 240; 200; 180; 170; 160)$ GeV, respectively.

The vacuum stability bound [24] comes from the requirement that the electroweak minimum of the effective potential is the deepest one for $|H| \leq \Lambda$. Remember that Λ is the scale up to which the Standard Model is assumed to be valid. For $|H| \gg v$ the mass terms in the effective potential are negligible compared to the self-interaction term and the vacuum stability requirement means that the Higgs self-interaction coupling is nonnegative $\bar{\lambda}(\mu) \geq 0$ for the scales $\mu \leq \Lambda$. Suppose that at scales $M \geq M_s$ we have some supersymmetric extension of the Standard Model. It should be noted that the most popular at present

is the minimal supersymmetric standard model (MSSM) [9] which predicts that the effective Higgs self-coupling constant for the standard model at the scale of supersymmetry breaking $M_s \equiv \Lambda$ has to obey the inequality

$$0 \leq \bar{\lambda}(M_s) = (\bar{g}_1^2(M_s) + \bar{g}_2^2(M_s))(\cos(2\varphi))^2/4 \leq (\bar{g}_1^2(M_s) + \bar{g}_2^2(M_s))/4\,. \tag{42}$$

So the assumption that the standard Weinberg–Salam model originates from its supersymmetric extension with the supersymmetry broken at scale M_s allows us to obtain nontrivial information about the low energy effective Higgs self-coupling constant in the effective potential $V = -M^2 H^+ H + \frac{\lambda}{2}(H^+ H)^2$ and hence to obtain nontrivial information about the Higgs boson mass. It should be noted that in nonminimal supersymmetric electroweak models, say in the model with additional gauge singlet σ, we have due to the $k\sigma H_1 i\tau_2 H_2$ term in the superpotential an additional term $k^2|H_1 i\tau_2 H_2|^2$ in the potential and as a consequence our boundary condition for the Higgs self-coupling constant has to be modified, namely

$$\bar{\lambda}(M_s) = \frac{1}{4}(\bar{g}_1^2(M_s) + \bar{g}_2^2(M_s))\cos^2(2\varphi) + \frac{1}{2}\bar{k}^2(M_s)\sin^2(2\varphi) \geq 0\,. \tag{43}$$

The boundary condition (43) depends on unknown coupling constant $\bar{k}^2(M_s)$. However it is very important to stress that for all nonminimal supersymmetric models broken to standard Weinberg–Salam model at scale M_s the effective Higgs self-coupling constant $\bar{\lambda}(M_s)$ is nonnegative which is a direct consequence of the nonnegativity of the effective potential in supersymmetric models. Therefore the vacuum stability requirement results naturally [25] if supersymmetry is broken at some high scale M_s and at lower scales the Weinberg–Salam model is an effective theory. For the Weinberg–Salam model with boundary condition (42) for the Higgs self-coupling constant $\bar{\lambda}(M_s)$ we have integrated numerically renormalization group equations in two-loop approximation. Also we took into account the one-loop correction to the Higgs boson mass (running Higgs boson mass $\bar{m}_h(\mu) = \sqrt{\bar{\lambda}(\mu)}v$ does not coincide with pole Higgs boson mass). Our results [25] for the Higgs boson mass $m_h(k, M_s, m_t^{\rm pole})$ for different values of M_s and $m_t^{\rm pole}$ are presented in the Table. Here $k = 0$ corresponds to the boundary condition $\bar{\lambda}(M_s) = 0$ (vacuum stability bound) and $k = 1$ corresponds to the boundary condition $\bar{\lambda}(M_s) = \frac{1}{4}(\bar{g}_1^2 + \bar{g}_2^2)$. So from the requirement that at some high scale M_s the MSSM is softly broken to the SM we find [25] that the Higgs boson mass lies in the interval

$$m_h(k = 0, M_s, m_t^{\rm pole}) \leq m_h \leq m_h(k = 1, M_s, m_t^{\rm pole}).$$

Table. The dependence of the Higgs boson mass $m_h(k, M_s, m_t^{\rm pole})$ on the values of M_s, $m_t^{\rm pole}$ and $k = 0, 1$. Everything except k is in GeV

$m_t^{\rm pole}$	165 k=0	165 k=1	170 k=0	170 k=1	175 k=0	175 k=1	180 k=0	180 k=1	185 k=0	185 k=1
$M_s = 10^3$	69	111	74	114	78	117	83	120	88	123
$M_s = 10^{3.5}$	81	117	86	120	92	124	98	128	104	132
$M_s = 10^4$	89	121	95	125	101	130	108	134	114	139
$M_s = 10^6$	105	129	113	135	121	141	129	147	137	153
$M_s = 10^8$	112	132	120	138	129	147	138	152	146	159
$M_s = 10^{10}$	115	133	124	140	133	147	142	154	151	161
$M_s = 10^{12}$	117	134	126	141	136	147	145	154	154	161
$M_s = 10^{14}$	118	134	127	141	132	148	147	156	156	164
$M_s = 10^{16}$	118	134	128	141	138	148	148	156	158	164

The accuracy in the determination of $m_h(k, M_s, m_t^{\rm pole})$ is related mainly to nonexact knowledge of $\alpha_3(M_Z)$ and it is estimated to be less than 3 GeV. For instance, for $m_t^{\rm pole} = 175$ GeV and $M_s = 10^8$ GeV we find that

$$129 \text{ GeV} \leq m_h \leq 147 \text{ GeV}.$$

Note that in the MSSM the mass of the lightest Higgs boson is less than $m_h \leq M_Z$ at tree-level. Radiative corrections can increase the mass of the lightest Higgs boson [26] up to 120 GeV provided the sparticle masses are less than 1 TeV. As it has been demonstrated in Refs. 27, in the Standard Model due to the vacuum stability condition the Higgs boson mass has to be heavier than ~ 120 GeV*. It means that by the measurement of the Higgs boson mass it would be possible to distinguish between SM and MSSM. In particular, the observation of the Higgs boson at LEP2 with a mass less than 110 GeV will be powerful nontrivial indication in favour of the existence of low energy broken supersymmetry.

3.3. Higgs Boson Mass Bound from Electroweak Precision Data. Indirect bound on the Higgs boson mass can be derived from the high-precision measurements of electroweak observables at LEP and elsewhere. The Standard Model is renormalizable only after including the top quark and the Higgs boson and as a consequence the electroweak observables are sensitive to the masses of these particles. The Fermi coupling can be rewritten as

$$\frac{G_F}{\sqrt{2}} = \frac{2\pi\alpha}{\sin^2(2\theta_W)M_Z^2}[1 + \Delta r_a + \Delta r_t + \Delta r_h]. \tag{44}$$

*Concrete details and rigorous statements are contained in [27].

The Δ terms take into account the radiative corrections: Δr_a describes the shift in the effective electromagnetic coupling constant; Δr_t takes into account the top quark contribution. The Δr_h denotes the Higgs boson contribution. This term depends logarithmically [28] on the Higgs boson mass and at leading order it reads

$$\Delta r_h = \frac{11 G_F M_W^2}{24\sqrt{2}\pi}[log(\frac{m_h^2}{M_W^2}) - \frac{5}{6}],\ (m_h^2 \gg M_W^2). \tag{45}$$

Although the sensitivity on the Higgs boson mass is only logarithmic, the increasing precision in the measurement of the electroweak observables allows one to derive constraints on the Higgs boson mass [29]

$$m_h = 71^{+75}_{-42} \pm 5 \text{ GeV}. \tag{46}$$

In other words it means that the Higgs boson should be relatively light with a mass less than $m_h < 220$ GeV at $95\,\%$ C.L. [29]. See, however, Ref. 30 where it has been shown on the base of the scale factor fit that 95 percent confidence level upper limit increases to as much as 750 GeV.

4. HIGGS BOSON DECAYS

The tree-level Higgs boson couplings to gauge bosons and fermions can be deduced from the Lagrangian (28), (29). Of these, the hW^+W^-, hZZ and $h\bar{\psi}\psi$ are the most important for the phenomenology. The partial decay width into fermion-antifermion pair is [31]

$$\Gamma(h \to \psi\bar{\psi}) = \frac{G_F m_\psi^2 m_h N_c}{4\pi\sqrt{2}}(1 - \frac{4m_\psi^2}{m_h^2})^{\frac{3}{2}}, \tag{47}$$

where N_c is the number of fermion colours. For $m_h \leq 2m_W$ Higgs boson decays mainly with ($\approx$ 90 percent) probability into b quark-antiquark pair and with ≈ 5 percent probability into τ lepton-antilepton pair. An account of higher order QCD corrections can be effectively taken into account in formula (47) for the Higgs boson decay into b quark-antiquark pair by the replacement of pole b-quark mass in formula (47) by the effective b-quark mass $\bar{m}_b(m_h)$. An account of higher order corrections leads to the formula [32] (see Fig. 2)

$$\Gamma(h \to Q\bar{Q}) = \frac{3G_F^2 m_h}{4\sqrt{2}\pi}\bar{m}_Q^2(m_h)[\Delta_{QCD} + \Delta_t], \tag{48}$$

$$\Delta_{QCD} = 1 + 5.67\frac{\alpha_s(m_h)}{\pi} + (35.94 - 1.36N_F)(\frac{\alpha_s(m_h)}{\pi})^2 +$$
$$+161.14 - 25.77N_F + 0.259N_F^2)(\frac{\alpha_s(m_h)}{\pi})^3, \tag{49}$$

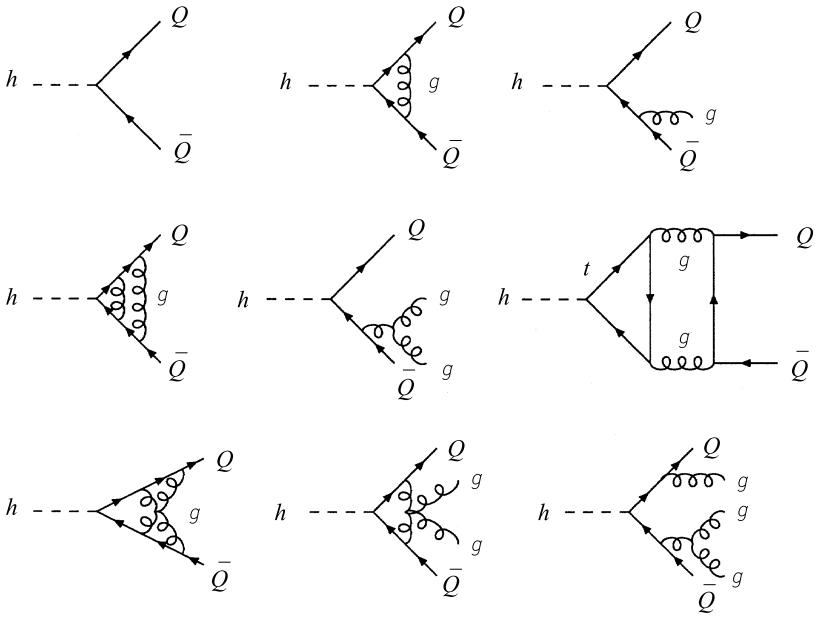

Fig. 2. Typical diagrams contributing to $h \to Q\bar{Q}$ at lowest order and one-, two- and three-loop QCD

$$\Delta_t = (\frac{\alpha_s(m_h)}{\pi})^2[1.57 - \frac{2}{3}\log\frac{m_h^2}{m_t^2} + \frac{1}{9}\log^2\frac{\bar{m}_Q^2(m_h)}{m_h^2}] \tag{50}$$

for the Higgs boson decay width to $Q = b, c$ quarks in the $\overline{MS}$ renormalization scheme. The relation between the perturbative quark pole mass m_Q and the $\overline{MS}$ running quark mass $\bar{m}_Q(m_Q)$ has the form [33]

$$\bar{m}_Q(m_Q) = \frac{m_Q}{1 + \frac{4}{3}\frac{\alpha_s(m_Q)}{\pi} + K_Q(\frac{\alpha_s(m_Q)}{\pi})^2}, \tag{51}$$

where numerically $K_t \approx 10.9$, $K_b \approx 12.4$ and $K_c \approx 13.4$. Electroweak corrections to heavy quarks and lepton decays are rather small [34] (less than 2 percent).

Higgs boson with $m_h \geq 2M_W$ will decay into pairs of gauge bosons (see Fig. 3) with the partial widths

$$\Gamma(h \to W^+W^-) = \frac{G_F m_h^3}{32\pi\sqrt{2}}(4 - 4a_W + 3a_W^2)(1 - a_W)^{\frac{1}{2}}\,, \tag{52}$$

$$\Gamma(h \to Z^0Z^0) = \frac{G_F m_h^3}{64\pi\sqrt{2}}(4 - 4a_Z + 3a_Z^2)(1 - a_Z)^{\frac{1}{2}}\,, \tag{53}$$

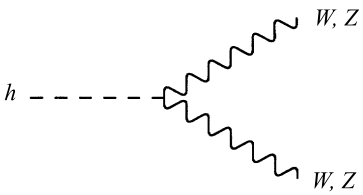

Fig. 3. Diagram contributing to $h \to \to VV$ $[V = W, Z]$

where $a_W = \frac{4M_W^2}{m_h^2}$ and $a_Z = \frac{4M_Z^2}{m_h^2}$. The electroweak corrections have been computed in Refs. 34. They are less than 5 percent in the intermediate region. The QCD corrections to the leading top mass corrections of $O(G_F m_t^2)$ have been calculated in Refs. 35.

In the heavy Higgs mass regime ($2m_Z \leq \leq m_h \leq 800$ GeV), the Higgs boson decays dominantly into gauge bosons. For example, for $m_h \gg 2m_Z$ one can find that

$$\Gamma(h \to W^+W^-) \simeq 2\Gamma(h \to ZZ) \simeq \frac{G_F m_h^3}{8\pi\sqrt{2}}\,. \tag{54}$$

The m_h^3 behaviour is a consequence of the longitudinal polarisation states of the W and Z. As m_h gets large, so does the coupling of h to the Goldstone bosons which have been eaten by the W and Z. However, the Higgs boson decay width to a pair of heavy quarks growth only linearly in the Higgs boson mass. Thus, for the Higgs masses sufficiently above $2m_Z$, the total Higgs boson width is well approximated by ignoring the Higgs boson decay to $t\bar{t}$ and including only two gauge boson modes. For heavy Higgs boson mass one can find that

$$\Gamma_{total}(h) \simeq 0.48\,\mathrm{TeV}(\frac{m_h}{1\,\mathrm{TeV}})^3\,. \tag{55}$$

For large Higgs boson mass higher order corrections due to the self-coupling of the Higgs boson are relevant, namely [36]

$$\Gamma(h \to VV) = \Gamma_{LO}(h \to VV)[1 + 2.8\kappa + 62.0\kappa^2], \tag{56}$$

where $\kappa = \frac{G_F m_h^2}{16\sqrt{2}\pi^2}$, $V = Z, W$.

Below threshold the decays into off-shell gauge particles are important. The decay width into single off-shell gauge boson has the form [37]

$$\Gamma(h \to VV^*) = \delta_V \frac{3G_F^2 M_V^4 m_h}{16\pi^3} R(\frac{M_V^2}{m_h^2}), \tag{57}$$

where $\delta_W = 1$, $\delta_Z = \frac{7}{12} - \frac{10}{9}\sin^2\theta_W + \frac{40}{27}\sin^4\theta_W$ and

$$R(x) = 3\frac{1 - 8x + 20x^2}{\sqrt{4x-1}}\arccos(\frac{3x-1}{2x^{3/2}}) -$$

$$-\frac{1-x}{2x}(2 - 13x + 47x^2) - \frac{3}{2}(1 - 6x + 4x^2)\log(x), \tag{58}$$

$x = \frac{M_V^2}{m_h^2}$. For Higgs boson mass slightly larger than the corresponding gauge boson mass the decay widths into pairs of off-shell gauge bosons play important role. The corresponding formulae can be found in Ref. 38.

It should be noted that there are a number of important Higgs boson couplings which are absent at tree-level but appear at one-loop level. Among them the couplings of the Higgs boson to two gluons and two photons are extremely important for the Higgs boson searches at supercolliders. One-loop induced Higgs coupling to two gluons is due to t-quark exchange in the loop (see Fig. 4) [39] and it leads to an effective Lagrangian

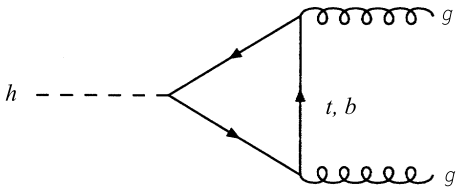

Fig. 4. Diagrams contributing to $h \to gg$ at lowest order

$$L_{hgg}^{eff} = \frac{g_2 \alpha_s N_g}{24\pi m_W} h G_{\mu\nu}^a G^{a\mu\nu} \tag{59}$$

for the interaction of the Higgs boson with gluons. At lowest order the partial decay width is given by [39]

$$\Gamma_{LO}(h \to gg) = \frac{G_F \alpha_s^2 m_h^3}{36\sqrt{2}\pi^3} |\sum_Q A_Q^h(\tau_Q)|^2, \tag{60}$$

$$A_Q^h(\tau) = \frac{3}{2}\tau[1 + (1-\tau)f(\tau)], \tag{61}$$

$$f(\tau) = \arcsin^2(\frac{1}{\sqrt{\tau}}) \text{ if } \tau \geq 1, \tag{62}$$

$$f(\tau) = -\frac{1}{4}\left[\ln\left(\frac{1+\sqrt{1-\tau}}{1-\sqrt{1-\tau}}\right) - i\pi\right]^2 \text{ if } \tau < 1. \tag{63}$$

The parameter $\tau_Q = \frac{4m_Q^2}{m_h^2}$ is defined by the pole mass m_Q of the heavy quark in the loop. For large quark mass $A_Q^h(\tau_Q) \to 1$. An account of the QCD radiative corrections (see Fig. 5) gives for $m_h^2 \ll 4m_Q^2$ [40]

$$\Gamma(h \to gg(q), q\bar{q}g) = \Gamma_{LO}[\alpha_s^{(N_F)}(m_h)][1 + (\frac{95}{4} - \frac{7}{6}N_F)\frac{\alpha_s^{(N_F)}(m_h)}{\pi}] \tag{64}$$

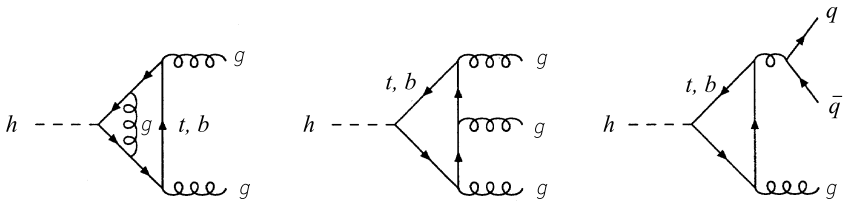

Fig. 5. Typical diagrams contributing to the QCD corrections to $h \to gg$

with $N_F = 5$ light quark flavours. It appears that radiative corrections are very large: the decay width is shifted by about (60–70) percent upwards in the most interesting mass region 100 GeV $\leq m_h \leq$ 500 GeV. Three-loop QCD corrections have been calculated in the limit of a heavy top quark [41]. They are positive and increase the full next leading order expression by 10 percent. Using the low-energy theorems it is possible to calculate easily the electroweak $O(G_F M_t^2)$ corrections to the leading order Higgs boson decay width into two gluons [42]

$$\Gamma(h \to gg) = \Gamma_{LO}(h \to gg)[1 + \frac{G_F M_t^2}{8\sqrt{2}\pi^2}]. \tag{65}$$

Numerically they are negligible.

Also very important is the one-loop induced Higgs boson coupling to two photons due to W and t-quark exchanges in the loop (see Fig. 6). The partial decay width can be written in the form

$$\Gamma(h \to \gamma\gamma) = \frac{G_F \alpha^2 m_h^3}{128\sqrt{2}\pi^3} |\sum_f N_{cf} e_f^2 A_f^h(\tau_f) + A_W^h(\tau_W)|^2, \tag{66}$$

where

$$A_f^h(\tau) = 2\tau[1 + (1-\tau)f(\tau)], \tag{67}$$

$$A_W^h(\tau) = -[2 + 3\tau + 3\tau(2-\tau)f(\tau)], \tag{68}$$

$\tau_i = \frac{4M_i^2}{m_h^2}$, $i = f, W$ and the function $f(\tau)$ is determined by the formulae (62), (63). The W loop gives the dominant contribution in the intermediate Higgs

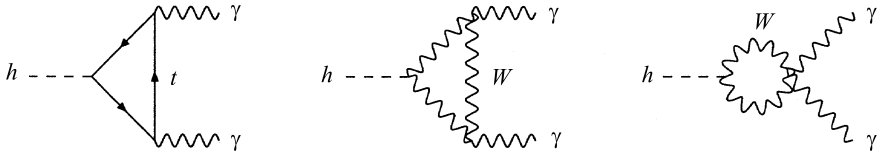

Fig. 6. Diagrams contributing to $h \to \gamma\gamma$ at lowest order

boson mass range. Two-loop QCD corrections to the quark loops have been calculated in [42]. QCD corrections rescale the lowest order by a factor that depends on the ratio of the Higgs boson and quark masses

$$A_Q^h(\tau_Q) \to A_Q^h(\tau_Q) \times [1 + C_h(\tau_Q)\frac{\alpha_s}{\pi}] \tag{69}$$

with $C_h(\tau_Q) \to -1$ for $m_h^2 \ll 4m_Q^2$. QCD corrections to the two photon Higgs boson decay width numerically are not very big, of $O(10)$ %. Electroweak corrections are less than 1 % [43].

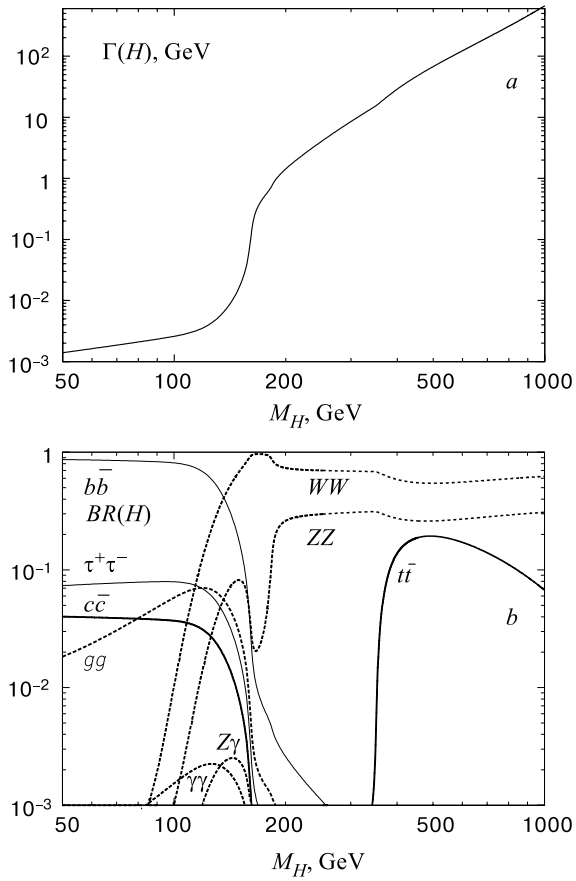

Fig. 7. *(a)* Total decay width (in GeV) of the SM Higgs boson as a function of its mass. *(b)* Branching ratios of the dominant decay modes of the SM Higgs particle. All relevant higher-order corrections are taken into account (Ref. 16) ($H \equiv h$)

5. HIGGS BOSON SEARCH AT LEP

The process that was used for the direct search for the Higgs boson at LEP1 was the Bjorken process [45]

$$e^+e^- \to Z \to (Z^* \to f\bar{f})h. \tag{70}$$

The differential decay width for the $Z \to (Z^* \to f\bar{f})h$ reaction normalized to $Z \to f\bar{f}$ decay is given by [46]

$$\frac{\Gamma(Z \to (Z^* \to f\bar{f})h)}{\Gamma(Z \to f\bar{f})} = \frac{\alpha}{4\pi \sin^2\theta_W \cos^2\theta_W} \frac{(1 - x + \frac{x^2}{12} + \frac{2r^2}{3})(x^2 - 4r^2)^{1/2}}{(x - r^2)^2 + (\Gamma_Z/M_Z)^2}, \tag{71}$$

where $x = 2E_h/M_Z$ and $r = m_h/M_Z$, the kinematical limits being $2r \le x \le \le 1 - r^2$. The energy of the Higgs boson E_h is related to the invariant mass of the fermion pair $M_{f\bar{f}}$ (i.e., the invariant mass of the virtual Z^* boson)

$$E_h = \frac{(M_Z^2 + m_h^2 - M_{f\bar{f}}^2)}{2M_Z}. \tag{72}$$

The Bjorken process with the decay of the virtual Z boson to $\mu^+\mu^-, e^+e^-, \nu\bar{\nu}$ pairs is used for the Higgs boson search. The decay of the Z^* to quark-antiquark pair is not useful due to large QCD background. The Higgs decay mode determines the Higgs signature in the detectors. Higgs bosons with low mass decay into e^+e^- and $\mu^+\mu^-$ pairs, for intermediate mass they decay into light hadrons and $\tau^+\tau^-$ pairs, and for high mass they decay mainly into a $b\bar{b}$ quark-antiquark pair. The combined limit of the four LEP1 experiments (ALEPH, DELPHI, L3 and OPAL) on the Higgs boson mass is [47]

$$m_h \ge 65.4 \text{ GeV}, \ 95\% \text{ C.L.} \tag{73}$$

At LEP2 with the total energy $\sqrt{s} = 130 - 200$ GeV the dominant Higgs production process * is $e^+e^- \to hZ$ («Higgs-strahlung» process). The corresponding cross section at tree-level is given by [48]

$$\sigma(e^+e^- \to hZ) = \frac{\pi\alpha^2\lambda^{1/2}(\lambda + 12sM_Z^2)[1 + (1 - 4\sin^2\theta_W)^2]}{192s^2 \sin^4\theta_W \cos^4\theta_W (s - M_Z^2)^2}, \tag{74}$$

where $\lambda \equiv (s - m_h^2 - M_Z^2)^2 - 4m_h^2M_Z^2$. One can see that for a fixed value of m_h, the cross section is maximal for $\sqrt{s} \approx m_Z + \sqrt{2}m_h$.

*The $e^+e^- \to WW$ and $e^+e^- \to ZZ$ fusions are still negligible at LEP2 energies

There are important differences between the Higgs boson searches at LEP1 and LEP2. The signal-to-background ratio is much better at LEP2. The large background rate at LEP1 required a very detailed simulation of detector effects and rare background reactions. The dominant hadronic Higgs boson signature ($Z^*h \to q\bar{q}q\bar{q}$) was useless at LEP1 due to large QCD background. While the expected Higgs boson production at LEP1 involved a real Z decaying into a Higgs boson and a virtual Z boson, at LEP2 the Higgs boson is produced in association with an on-shell Z boson. This additional information about the final-state Z boson gives rise to better Higgs boson mass reconstruction and greater sensitivity for a Higgs boson signal due to better background rejection.

Final state particles in the analysed Higgs boson channels at LEP2 are

$$e^+e^- \to (Z \to q\bar{q}, \nu\bar{\nu}, e^+e^-, \mu^+\mu^-, \tau^+\tau^-)(h \to b\bar{b}, \tau^+\tau^-). \tag{75}$$

Thus the three typical signatures are:

(a) two b-jets + a charged lepton pair ($Z \to \mu^+\mu^-(e^+e^-)$, $h \to b\bar{b}$),

(b) two b-jets plus missing transverse energy ($Z \to \nu\bar{\nu}$, $h \to b\bar{b}$),

(c) four jets with at least two b-jets or two τ-jets ($Z \to q\bar{q}$, $h \to b\bar{b}$ or $(hZ \to q\bar{q}\tau^+\tau^-)$).

The Standard Model background to these signatures is well known and it is under control [48, 49]. For example, the Higgs boson production cross section at $\sqrt{s} = 189$ GeV for $m_h = 95$ GeV is 0.18 pb, whereas the main background cross sections are 98 pb ($e^+e^- \to q\bar{q}$), 16 pb ($e^+e^- \to WW$), 0.62 pb ($e^+e^- \to ZZ$).

1998 LEP2 run with full energy $\sqrt{s} = 189$ GeV and with $L \approx 170\ \mathrm{pb}^{-1}/\exp$ allowed one to deduce the following 95 % C.L. lower Higgs boson mass bounds [50–54]

$$m_h > 90.2 \text{ GeV (ALEPH)},$$

$$m_h > 95.2 \text{ GeV (DELPHI)},$$

$$m_h > 95.3 \text{ GeV (L3)},$$

$$m_h > 91.0 \text{ GeV (OPAL)}.$$

Note that an additional account of 1999 data with integrated luminosities 29 fb^{-1} and 69.5 fb^{-1} at $\sqrt{s} = 191.6$ GeV and $\sqrt{s} = 195.6$ GeV allowed the ALEPH Collaboration to deduce the Higgs boson mass bound $m_h > 98.8$ GeV [55]. Recent preliminary combined limit of 4 LEP2 experiments with $\sqrt{s} \leq$ ≤ 195.6 GeV [56] gives $m_h > 102.6$ GeV at 95 % C.L.

LEP2 run with total energy $\sqrt{s} = 200$ GeV and with total luminosity $L_t =$ $= 200\ \mathrm{pb}^{-1}$ for each experiment will be able to discover standard Higgs boson with a mass up to 107 GeV [57].

6. HIGGS BOSON PRODUCTION AT HADRON SUPERCOLLIDERS

Typical processes that can be exploited to produce Higgs bosons in hadron supercolliders are:

gluon fusion: $gg \to h$,

WW, ZZ fusion: $W^+W^-, ZZ \to h$,

«Higgs-strahlung» off W, Z: $q\bar{q}W, Z \to W, Z + h$,

Higgs-bremsstrahlung off top: $q\bar{q}, gg \to t\bar{t} + h$.

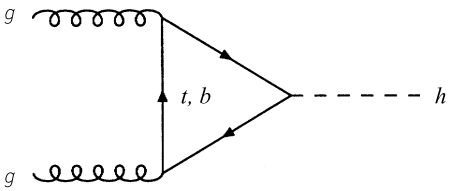

Fig. 8. Diagram contributing to the formation of Higgs bosons in gluon-gluon collisions at lowest order

Gluon fusion plays a dominant role at the LHC throughout the entire Higgs boson mass range of the SM whereas the WW/ZZ fusion process becomes increasingly important with Higgs boson rising. The last two reactions are important only for light Higgs boson masses.

The gluon-fusion mechanism [58] (see Fig. 8)

$$pp \to gg \to h \tag{76}$$

is the dominant production mechanism of the Higgs boson at the LHC for Higgs boson mass up to 1 TeV. The gluon coupling to the Higgs boson in the SM is mediated by triangular loops of top and bottom quarks. The corresponding form factor approaches a nonzero value for large loop-quark masses. At lowest order the partonic cross section can be expressed by the gluonic width of the Higgs boson

$$\hat{\sigma}_{LO}(gg \to h) = \sigma_0 m_h^2 \delta(\hat{s} - m_h^2), \tag{77}$$

$$\sigma_0 = \frac{\pi^2}{8m_h^2}\Gamma_{LO}(h \to gg) = \frac{G_F \alpha_s^2}{288\sqrt{2}\pi}|\sum_Q A_Q^h(\tau_Q)|^2, \tag{78}$$

where $\tau_Q = \frac{4M_Q^2}{m_h^2}$, $\hat{s}$ denotes the partonic system of mass energy squared and the form factor A_Q^h is determined by the formulae (62), (63). In the narrow-width approximation hadronic cross section can be written in the form

$$\sigma_{LO}(pp \to h + ...) = \sigma_0 \tau_h \frac{dL^{gg}}{d\tau_h}, \tag{79}$$

where $\frac{dL^{gg}}{d\tau_h}$ denotes gg luminosity of the pp collider with $\tau_h = \frac{m_h^2}{s}$. The QCD corrections to the gluon fusion process (see Fig. 9) are essential [59]. They

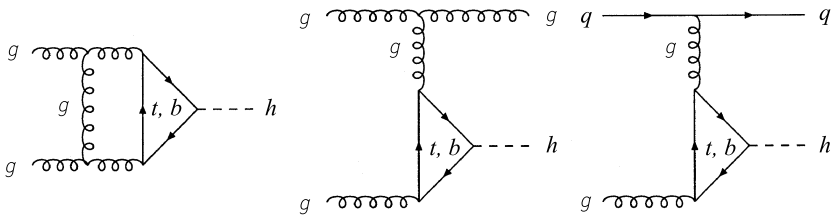

Fig. 9. Typical diagrams contributing to the virtual/real QCD corrections to $gg \to h$

stabilize the theoretical predictions for the cross section when the renormalization and factorisation scales are varied. Moreover, they are large and positive, thus increasing the production cross section for Higgs bosons. The QCD corrections consist of virtual corrections to the basic process $gg \to h$ and of real corrections due to reactions $gg \to hg$, $qq \to hq$ and $q\bar{q} \to hg$. The virtual corrections rescale the lowest-order fusion cross section with a coefficient that depends only on the ratios of the Higgs and quark masses. The next-to-leading order for the hadronic cross section can be represented in the form [59]

$$\sigma(pp \to h + ...) = \sigma_0[1 + C\frac{\alpha_s}{\pi}]\tau_h \frac{dL^{gg}}{d\tau_h} + \Delta\sigma_{gg} + \Delta\sigma_{qg} + \Delta\sigma_{q\bar{q}}. \qquad (80)$$

The calculation has been performed [59] in the $\overline{MS}$ scheme. The mass M_Q is identified with the pole quark mass and the renormalization scale in α_s and the factorisation scale of the parton densities is fixed at the Higgs boson mass. The coefficient $C(\tau_Q)$ denotes the finite part of the virtual two-loop corrections. The finite parts of the hard contributions from gluon radiation in gg scattering , gq scattering and $q\bar{q}$ annihilation are presented in the form [59]

$$\Delta\sigma_{gg} = \int_{\tau_h}^{1} d\tau \frac{dL^{gg}}{d\tau} \times \frac{\alpha_s}{\pi}\sigma_0[-zP_{gg}(z)\log z + d_{gg}(z,\tau_Q) + \qquad (81)$$
$$+ 12[(\frac{\log(1-z)}{(1-z)} - z[2 - z(1-z)]\log(1-z)]]\,,$$

$$\Delta\sigma_{gq} = \int_{\tau_h}^{1} \sum_{q,\bar{q}} \frac{dL^{gq}}{d\tau} \times \frac{\alpha_s}{\pi}\sigma_0[-\frac{z}{2}P_{gq}(z)\log\frac{z}{(1-z)^2} + d_{gq}(z,\tau_Q)]\,, \qquad (82)$$

$$\Delta\sigma_{q\bar{q}} = \int_{\tau_h}^{1} d\tau \sum_{q} \frac{dL^{q\bar{q}}}{d\tau} \times \frac{\alpha_s}{\pi}\sigma_0 d_{q\bar{q}}(z,\tau_Q)\,, \qquad (83)$$

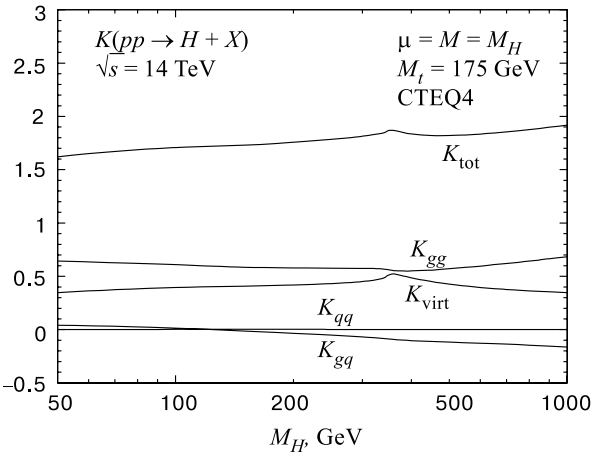

Fig. 10. K factors of the QCD-corrected gluon-fusion cross section $\sigma(pp \to h + X)$ at the LHC with c.m. energy $\sqrt{s} = 14$ TeV. The renormalization and factorisation scales have been identified with the Higgs mass, and CTEQ4 parton densities have been adopted (Ref. 16) ($H \equiv h$)

where $z = \tau_h/\tau = m_h^2/\hat{s}$, P_{gg} and P_{gq} are Altarelli–Parisi splitting functions. In the heavy quark limit one can find that [59]

$$C(\tau_Q) \to \pi^2 + 5.5, \tag{84}$$

$$d_{gg}(z, \tau_Q) \to -5.5(1-z)^3, \tag{85}$$

$$d_{gq}(z, \tau_Q) \to \frac{2}{3}z^2 - (1-z)^2, \tag{86}$$

$$d_{q\bar{q}}(z, \tau_Q) \to \frac{32}{27}(1-z)^3. \tag{87}$$

The size of the radiative corrections can be parametrised by defining the K factor as $K = \sigma_{NLO}/\sigma_{LO}$. The results of the calculations are presented in Fig. 10. The virtual and the real corrections for the gg collisions are the most important, they are large and positive. After including higher order QCD corrections the dependence of the cross section on the renormalization and factorisation scales is reduced from the level of $O(1)$ to a level of about $O(0.2)$.

The theoretical prediction for the Higgs boson production cross section is presented in Fig. 11 for the LHC as a function of the Higgs boson mass. The cross section decreases with increasing of the Higgs boson mass mainly due to the decrease of gg partonic luminosity for large invariant masses.

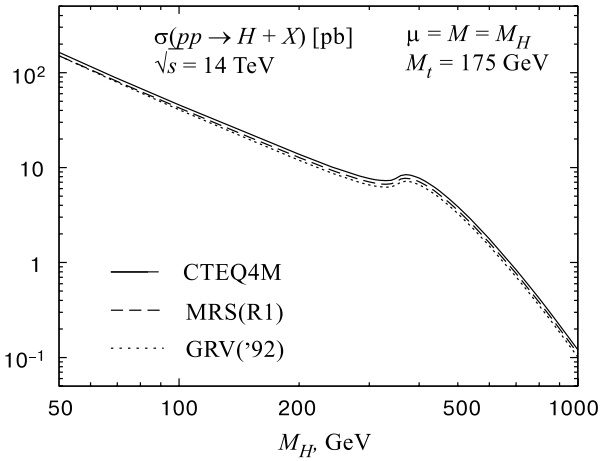

Fig. 11. The cross section for the production of Higgs bosons; three different sets of parton densities are shown (CTEQ4M, MRS(R1) and GRV('92)) (Ref. 16) ($H \equiv h$)

The second important process for the Higgs boson production at the LHC is vector-boson fusion (see Fig. 12), $W^+W^-(ZZ) \to h$ [60]. For large Higgs boson mass this mechanism becomes competitive to gluon fusion; for intermediate masses the cross section is smaller by about an order of magnitude. For large Higgs boson mass the W and Z bosons are predominantly longitudinally polarised. At high energies, the equivalent particle spectra of the longitudinal W, Z bosons in quark beam have the form [16]

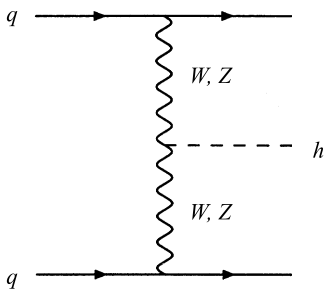

Fig. 12. Diagram contributing to $qq \to qqV^*V^* \to qqh$ at lowest order

$$f_L^W(x) = \frac{G_F M_W^2}{2\sqrt{2}\pi^2} \frac{1-x}{x}\,, \tag{88}$$

$$f_L^Z(x) = \frac{G_F M_Z^2}{2\sqrt{2}\pi^2} [(I_3^q - 2e_q \sin^2\theta_W)^2 + (I_3^q)^2] \frac{1-x}{x}\,, \tag{89}$$

where x is the fraction of energy transferred from the quark to the W, Z boson in the splitting process $q \to q + W/Z$. The WW and ZZ luminosities are presented in the form:

$$\frac{dL^{WW}}{d\tau_W} = \frac{G_F^2 M_W^4}{8\pi^4} \left[2 - \frac{2}{\tau_W} - \frac{1+\tau_W}{\tau_W} \log \tau_W \right]\,, \tag{90}$$

$$\frac{dL^{ZZ}}{d\tau_Z} = \frac{G_F^2 M_Z^4}{8\pi^4}[(I_3^q - 2e_q \sin^2\theta_W)^2 + (I_3^q)^2][(I_3^{q'} - \tag{91}$$
$$-2e_{q'} \sin^2\theta_W)^2 + (I_3^{q'})^2] \cdot [2 - \frac{2}{\tau_Z} - \frac{1+\tau_Z}{\tau_Z}\log\tau_Z] ,$$

where $\tau_V = \frac{M_{VV}^2}{s}$. Denoting the parton cross section for $WW, ZZ \to h$ by $\hat{\sigma}_0$ with

$$\hat{\sigma}_0(VV \to h) = \sigma_0 \delta(1 - m_h^2/\hat{s}), \tag{92}$$

$$\sigma_0 = \sqrt{2}\pi G_F , \tag{93}$$

the cross sections for the Higgs boson production in quark-quark and hadron-hadron collisions are presented in the form [16]

$$\hat{\sigma}(qq \to qqh) = \frac{dL^{VV}}{d\tau_V}\sigma_0 , \tag{94}$$

$$\sigma(qq' \to VV \to h) = \int_{m_h^2/s}^1 d\tau \sum_{q,q'} \frac{dL^{qq'}}{d\tau}\hat{\sigma}(qq' \to qq' h; \hat{s} = \tau s) . \tag{95}$$

«Higgs-strahlung» $q\bar{q} \to V^* \to Vh$ $(V = W, Z)$ (see Fig. 13) is a very important process for the search of light Higgs boson at the TEVATRON and LHC. Though the cross section is smaller than for gluon fusion, leptonic decays of electroweak vector bosons are extremely useful to filter Higgs boson signal from a huge background. The corresponding formulae for the cross section are contained in [61].

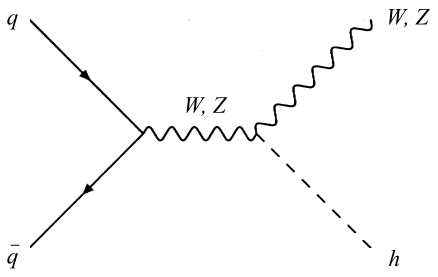

Fig. 13. Diagram contributing to $qq \to \to V^* \to Vh$ at lowest order

The process $gg, q\bar{q} \to t\bar{t}h$ (see Fig. 14) is relevant for small Higgs boson masses. The analytical expression for the parton cross section is quite involved [62]. Note that Higgs boson bremsstrahlung off top quarks is an interesting process for measurements of the fundamental $h\bar{t}t$ Yukawa coupling. The cross section $\sigma(pp \to t\bar{t}h)$ is directly proportional to the square of this coupling constant.

One can say that three classes of processes can be distinguished. The gluon fusion of Higgs boson is a universal process, dominant over the entire Higgs boson mass range. «Higgs-strahlung» of electroweak W, Z bosons or top quarks

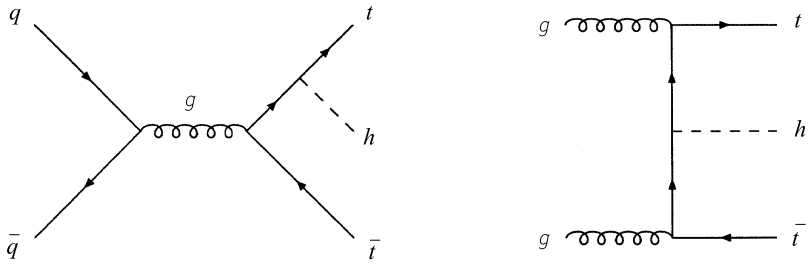

Fig. 14. Typical diagrams contributing to $q\bar{q}/gg \to ht\bar{t}$ at lowest order

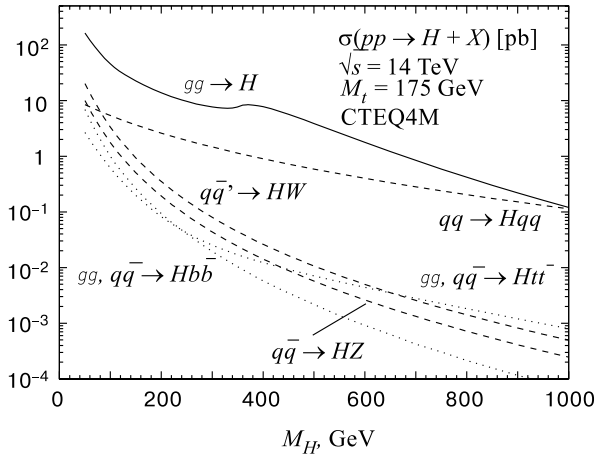

Fig. 15. Higgs production cross sections at the LHC for various production mechanisms as a function of the Higgs mass. The full QCD-corrected results for the gluon fusion $gg \to h$, vector-boson fusion $qq \to VVqq \to hqq$, vector-boson bremsstrahlung $q\bar{q} \to V^* \to hV$ and associated production $gg, q\bar{q} \to ht\bar{t}, hb\bar{b}$ are shown [16] ($H \equiv h$)

is important for light Higgs boson. The WW/ZZ fusion channel, by contrast, becomes rather important in the upper part of the Higgs boson mass. An overview of the production cross section for the Higgs boson at the LHC is presented in Fig. 15.

7. SEARCH FOR THE HIGGS BOSON AT TEVATRON

It is expected [63, 64] that upgraded Fermilab Tevatron (TEV22) will start in the 2000 year with the full energy $\sqrt{s} = 2$ TeV, and the full luminosity for each experiment during 3 years of exploitation will be $L_t = 2\ \mathrm{fb}^{-1}$. There are

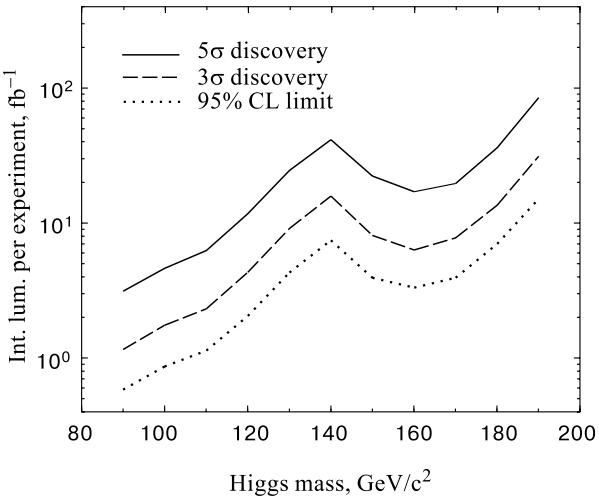

Fig. 16. Luminosity required as a function of Higgs mass to achieve different levels of sensitivity to the standard-model Higgs boson. The upper curve corresponds to a 5 σ discovery, the middle to a 3 σ signal and the lower to a 95% exclusion limit. These limits require two experiments, Bayesian statistics are used to combine the channels and include the improved sensitivity which would come from multivariate analysis techniques (Ref. 64)

also plans to increase luminosity to have $L_t = 30$ fb^{-1} (TEV33) by 2006. The most interesting process for the search for standard Higgs boson at the Tevatron is «Higgs-strahlung» off W, Z bosons $q\bar{q} \to W^*/Z^* \to W/Z + h$. For the Higgs boson mass 100 GeV $\leq m_h \leq$ 140 GeV the cross section is between 0.5 pb and 0.1 pb. The QCD corrections for «Higgs-strahlung» coincide with those of the Drell–Yan process and increase tree-level cross section approximately by 30 percent. The most promising signatures are

$$p\bar{p} \to (h \to b\bar{b})(W \to l\nu, \text{jets}) + \text{anything}, \tag{96}$$

$$p\bar{p} \to (h \to b\bar{b})(Z \to l^+l^-, \nu\bar{\nu}) + \text{anything}. \tag{97}$$

The $b\bar{b}$ decay of the Higgs boson adds powerful background rejection based on b-tagging especially at low Higgs boson mass, below ~ 130 GeV where that decay dominates. Other very promising signature [65] is the use of $h \to W^*W^* \to$ $\to l\bar{\nu}\bar{l}\nu$ decay mode with the dominant gluon-gluon Higgs boson fusion production mechanism. The main conclusion of Ref. 65 is that for an integrated luminosity of 30 fb^{-1} the Higgs boson signal should be observable at a 3σ level or better for the mass range 145 GeV $\leq m_h \leq$ 180 GeV and for 95 % percent confidence level exclusion, the mass reach is 135 GeV $\leq m_h \leq$ 190 GeV. One can say that at TEV33 run with the full luminosity $L_t = 30$ fb^{-1} it would

be possible to discover the Higgs boson at $\geq 3\sigma$ level at least with a mass up to (180–190) GeV [63–65]. The Higgs boson discovery potential of Tevatron Collider is shown in Fig.16.

8. LHC DETECTORS

The LHC (Large Hadron Collider) [66–69] which will be the biggest particle accelerator complex ever built in the world will accelerate two proton beams with the total energy $\sqrt{s} = 14$ TeV. At low luminosity stage (first two-three years of operation) the luminosity is planned to be $L_{\rm low} = 10^{33}\ {\rm cm}^{-2}{\rm s}^{-1}$ with total luminosity $L_{\rm tot} = 10^4\ {\rm pb}^{-1}$ per year. At high luminosity stage the luminosity is planned to be $L_{\rm high} = 10^{34}\ {\rm cm}^{-2}{\rm s}^{-1}$ with total luminosity $L_{\rm tot} = 10^5\ {\rm pb}^{-1}$ per year. The LHC will start to work in the 2005 year. There are planned to be two big general purpose detectors at LHC CMS (Compact Muon Solenoid) and ATLAS (A Toroidal LHC Apparatus).

The scientific program at the LHC consists in many goals [66–69]. One of the most important tasks for the LHC is the quest for the origin of the spontaneous symmetry-breaking mechanism in the electroweak sector of the SM. As it has been mentioned before, all the renormalizable models of electroweak interactions are based on the use of the gauge symmetry breaking. As a consequence of the electroweak symmetry breaking and the renormalizability of the theory there must be neutral scalar particle (Higgs boson) in the spectrum. So the discovery of the Higgs boson will be the check of the spontaneous symmetry breaking and the renormalizability of the theory and therefore there are no doubts that the Higgs boson discovery is the supergoal number 1 for the LHC. The Higgs boson search is therefore used as a first benchmark for the detector optimisation for both CMS and ATLAS. For the SM Higgs boson, the detector has to be sensitive to the following processes in order to cover the full mass range above the expected LEP2 discovery limit of $(105 - 110)$ GeV:

A. $h \to \gamma\gamma$ mass range 90 GeV $\leq m_h \leq$ 150 GeV,

B. $h \to b\bar{b}$ from $Wh, Zh, t\bar{t}h$ using $l^{\pm}(l^{\pm} = e^{\pm}$ or $\mu^{\pm})$-tag and b-tagging in the mass range 80 GeV $\leq m_h \leq$ 100 GeV,

C. $h \to ZZ^* \to 4l^{\pm}$ for the mass range 130 GeV $\leq m_h \leq 2m_Z$,

D. $h \to ZZ \to 4l^{\pm}, 2l^{\pm}2\nu$ for the mass range $m_h \geq 2m_Z$,

E. $h \to WW, ZZ \to l^{\pm}\nu$ 2 jets, $2l^{\pm}$ 2 jets, using tagging of forward jets for m_h up to 1 TeV.

In minimal supersymmetric extension of the standard model (MSSM) there is a family of Higgs particles ($H^{\pm}, h, H$ and A). So in addition to the standard Higgs boson signatures the MSSM Higgs searches are based on the following processes:

F. $A \to \tau^+\tau^- \to e\mu$ plus $\nu's$, or $A \to \tau^+\tau^- \to l^{\pm}$ plus hadrons plus $\nu's$,

G. $H^{\pm} \to \tau^{\pm}\nu$ from $t\bar{t} \to H^{\pm}W^{\mp}b\bar{b}$ and $H^{\pm} \to 2$ jets, using a $l^{\pm}$- tag and b-tagging.

The observable cross sections for most of those processes are small (1–100) pb over a large part of the mass range. So it is necessary to work at high luminosity and to maximise the detectable rates above backgrounds by high-resolution measurements of electrons, muons and photons.

For the $H^{\pm}$ and A signatures in the case of the MSSM, high performance detector capabilities are required in addition for the measurements which are expected to be the best achieved at initial luminosities with a low level of overlapping events, namely secondary vertex detection for τ-leptons and b-quarks, and high resolution calorimetry for jets and missing transverse energy $E_T^{\rm miss}$.

The second supergoal of the LHC project is the supersymmetry discovery, i.e., the detection of superparticles. Here the main signature are the missing transverse energy events which are the consequence of undetected lightest stable supersymmetric particles (LSP) predicted in supersymmetric models with R-parity conservation. Therefore it is necessary to set stringent requirements for the hermeticity and $E_T^{\rm miss}$ capability of the detector. Also the search for new physics different from supersymmetry (new gauge bosons $W^{'}$ and $Z^{'}$, new Higgs bosons with big Yukawa couplings, etc.) at LHC requires high resolution lepton measurements and charge identification even in the p_T range of a few TeV. Other possible signature of new physics (compositeness) can be provided by very high p_T jet measurements. An important task of LHC is the study of b- and t-physics. Even at low luminosities the LHC will be a high rate beauty and top quark factory. The main emphasis in B-physics is the precise measurement of CP-violation in the B_d^0 system and the determination of the Kobayashi–Maskawa angles. Besides investigations of $B\bar{B}$ mixing in the B_S^0 system, rare B decays are also very important. Precise secondary vertex determination, full reconstruction of final states with relatively low-p_T particles, an example being $B_d^0 \to J/\Psi K_S^0$ followed by $J/\Psi \to l^+l^-$ and $K_S^0 \to \pi^+\pi^-$, and low-p_T lepton first-level triggering capability are all necessary. In addition to running as a proton-proton collider, LHC will be used to collide heavy ions at a centre of mass energy 5.5 TeV per nucleon pair. The formation of quark-gluon plasma in the heavy ion collisions is predicted to be signalled by a strong suppression of $\Upsilon^{'}$ and $\Upsilon^{''}$ production relative to Υ production when compared with pp collisions. The CMS and ATLAS detectors will be used to detect low momentum muons produced in heavy ion collisions and reconstruct Υ-, $\Upsilon^{'}$- and $\Upsilon^{''}$-meson production. Therefore the basic design considerations for both ATLAS and CMS are the following:

1. very good electromagnetic calorimetry for electron and photon identification and measurements,

2. good hermetic jet and missing E_T-calorimetry,

3. efficient tracking at high luminosity for lepton momentum measurements,

for b-quark tagging, and for enhanced electron and photon identification, as well as tau and heavy-flavour vertexing and reconstruction capability of some B-decay final states at lower luminosity,

4. stand-alone, precision, muon-momentum measurement up to the highest luminosity, and very low-p_T trigger capability at lower luminosity,

5. large acceptance in η coverage.

8.1. Brief Description of CMS Subdetectors [67] . The CMS detector consists of inner detector (tracker), electromagnetic calorimeter, hadron calorimeter, muon spectrometer and trigger. A schematic view of the CMS detector is shown in Fig. 17.

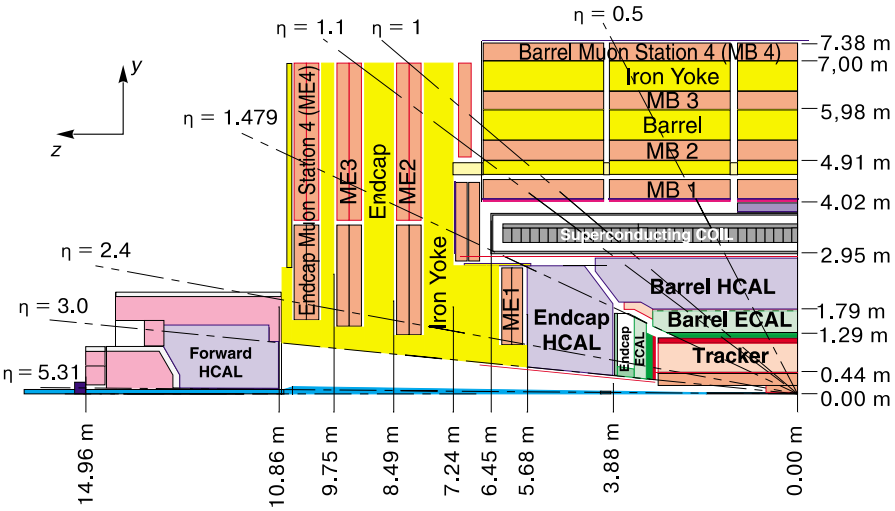

Fig. 17. Longitudinal view of the CMS detector

Tracker. The design goal of the central tracking system is to reconstruct isolated high-p_T tracks with an efficiency better than 95 percent, and high-p_T tracks within jets with an efficiency of better than 90 percent over the rapidity $|\eta| \leq 2.6$. The momentum resolution required for isolated charged leptons in the central rapidity region is $\frac{\delta p_T}{p_T} = 0.1 p_T$ (p_T in TeV). This will allow the measurement of the lepton charge up to $p_T = 2$ TeV. It is also very important for tracking system to perform efficient b- and τ-tagging. The tracker system consists of silicon pixels, silicon and gas microstrip detectors (MSGS) which provide precision momentum measurements and ensure efficient pattern of recognition even at the highest luminosity. A silicon pixel detectors consist of two barrel layers and three endcap layers and it is placed close to the beam pipe with the tasks of:

a. assisting in pattern recognition by providing two or three true space points per track over the full rapidity range in the main tracker,

b. improving the impact parameter resolution for b-tagging,

c. allowing 3-dimensional vertex reconstruction by providing a much improved Z-resolution in the barrel part.

The silicon microstrip detector is required to have a powerful vertex finding capability in the transverse plane over a large momentum range for b-tagging and heavy quark physics and must be able to distinguish different interaction vertices at high luminosity. The CMS silicon microstrip detector is subdivided into barrel and forward parts, meeting at $|\eta| = 1.8(\eta \equiv -\ln(\tan(\frac{\theta}{2}))$, provided at least 3 measuring points on each track for $|\eta| \leq 2.6$. The microstrip gas chambers provide a minimum of 7 hits for high-p_T tracks. The track finding efficiency in the tracker is 98 percent for $p_T \geq 5$ GeV. The charged particle momentum resolution depends on the η and p_T of charged particle and for $p_T = 100$ GeV and $|\eta| \leq 1.75$ it is around 2 percent. Impact parameter resolution also depends on p_T and η and for 10 GeV $\leq p_T \leq$ 100 GeV and $|\eta| \leq 1.3$ in transverse plane it is around 100 μm. The b-tagging efficiency from $\bar{t}t$ decays is supposed to be better than 30 percent. A significant impact parameter resolution can be used to tag τ-leptons. It could be useful in searches such as SUSY Higgs boson decays $A, H, h \rightarrow \tau\tau \rightarrow e + \mu + X$(or $l + \text{hadrons}$). These leptons (hadrons) originate from secondary τ vertices while in the backgrounds from $\bar{t}t \rightarrow Wb + W\bar{b} \rightarrow e + \mu + X$ and $WW \rightarrow e + \mu + X$ they originate from the primary vertex. It is possible to have the efficiency for the signal ≈ 50 percent while for the background channels it is ≈ 3 percent.

ECAL. The barrel part of the electromagnetic calorimeter covers the rapidity intervals $|\eta| \leq 1.56$. The endcaps cover the intervals $1.65 \leq |\eta| \leq 2.61$. The gaps between the barrel and the endcaps are used to route the services of the tracker and preshower detectors. The barrel granularity is 432 fold in ϕ and 108×2-fold in η. A very good intrinsic energy resolution given by

$$\frac{\sigma}{E} = \frac{0.02}{\sqrt{E}} \oplus 0.005 \oplus \frac{0.2}{E} \tag{98}$$

is assumed to be for electrons and photons with a $PbWO_4$ crystal ECAL. The physics process that imposes the strictest performance requirements on the electromagnetic calorimeter is the intermediate mass Higgs boson decaying into two photons. The main goal here is to obtain very good diphoton mass resolution. The mass resolution has terms that depend on the resolution in energy (E_1, E_2) and the two-photon angular separation (θ) and it is given by

$$\frac{\sigma_M}{M} = \frac{1}{2}\left[\frac{\sigma_{E_1}}{E_1} \oplus \frac{\sigma_{E_2}}{E_2} \oplus \frac{\sigma_\theta}{(\tan(\frac{\theta}{2}))}\right], \tag{99}$$

where $\oplus$ denotes a quadratic sum, E is in GeV and θ is in radians. For the Higgs two-photon decay at LHC the angular term in the mass resolution can become important, so it is necessary to measure the direction of the photons using the information from the calorimeter alone. In the barrel region $|\eta| \leq 1.56$ angular resolution is supposed to be $\sigma_\theta \leq \frac{50\text{mrad}}{\sqrt{E}}$. Estimates give the following diphoton mass resolution for $h \to \gamma\gamma$ channel ($m_h = 100$ GeV):

$\delta m_{\gamma\gamma} = 475$ MeV (low luminosity $L = 10^{33}$ cm^{-2}s^{-1}),

$\delta m_{\gamma\gamma} = 775$ MeV (high luminosity $L = 10^{34}$ cm^{-2}s^{-1}).

HCAL. The hadron calorimeter surrounds the electromagnetic calorimeter and acts in conjunction with it to measure the energies and directions of particle jets, and to provide hermetic coverage for measurement of the transverse energy. The pseudorapidity range ($|\eta| \leq 3$) is covered by the barrel and endcap hadron calorimeters which sit inside the 4T magnetic field of CMS solenoid. In the central region around $\eta = 0$ a hadron shower 'tail catcher' is installed outside the solenoid coil to ensure adequate sampling depth. The active elements of the barrel and endcap hadron calorimeter consist of plastic scintillator tiles with wave length-shifting fibre readout. The pseudorapidity range ($3.0 \leq \eta \leq 5.0$) is covered by a separate very forward calorimeter. The hadron calorimeter must have good hermeticity, good transverse granularity, moderate energy resolution and sufficient depth for hadron shower containment. The physics programme requires good hadron resolution and segmentation to detect narrow states decaying into pairs of jets. The dijet mass resolution includes contributions from physics effects such as fragmentation as well as detector effects such as angular and energy resolution. The energy resolution is assumed to be:

$$\frac{\Delta E}{E} = \frac{0.6}{\sqrt{E}} \oplus 0.03 \tag{100}$$

for $|\eta| \leq 1.5$ and segmentation $\Delta\eta \times \Delta\Phi = 0.1 \times 0.1$.

The dijet mass resolution is approximately the following:

1. $(10 - 15)\%$ for 50 GeV $\leq p_T \leq 60$ GeV and $m_{ij} = m_Z$,
2. $(5 - 10)\%$ for 500 GeV $\leq p_T \leq 600$ GeV and $m_{ij} = m_Z$.

The expected energy resolution for jets in the very forward calorimeter is parametrised by:

$$\frac{\sigma_{E_{\text{jet}}}}{E_{\text{jet}}} = \frac{1.28 \pm 0.1}{\sqrt{E_{\text{jet}}}} \oplus (0.02 \pm 0.01)\,. \tag{101}$$

The expected missing transverse energy resolution in the CMS detector with very forward $2.5 \leq \eta \leq 4.7$ coverage is

$$\frac{\sigma_t}{\sum E_t} = \frac{0.55}{\sqrt{\sum E_t}}\,, \tag{102}$$

(E_t in GeV). In the absence of the very forward calorimeter, the missing transverse energy resolution would be nearly three times worse.

Muon system. At the LHC the effective detection of muons from Higgs bosons, W, Z and $t\bar{t}$ decays requires coverage over a large rapidity interval. Muons from pp collisions are expected to provide clean signatures for a wide range of new physics processes. Many of these processes are expected to be rare and will require the highest luminosity. The goal of the muon detector is to identify these muons and to provide a precision measurement of their momenta from a few GeV to a few TeV. The barrel detector covers the region $|\eta| \leq 1.3$. The endcap detector covers the region $1.3 \leq |\eta| \leq 2.4$. The muon detector should fulfil three basic tasks: muon identification, trigger and momentum measurement. The muon detector is placed behind ECAL and the coil. It consists of four muon stations interleaved with the iron return yoke plates. The magnetic flux in the iron provides the possibility of an independent momentum measurement. The barrel muon detector is based on a system of 240 chambers of drift tubes arranged in four concentric stations. In the endcap regions, the muon detector comprises four muon stations. The muon detector has the following functionality and performance:

1. geometric coverage: pseudorapidity coverage up to $|\eta| = 2.4$ with the minimum possible acceptance loses due to gaps and dead areas,

2. transverse momentum resolution for the muon detector alone for $0 \leq |\eta| \leq 2 : \frac{\Delta p_T}{p_T} = 0.06 - 0.1$ for $p_T = 10$ GeV, $0.07 - 0.2$ for $p_T = 100$ GeV and $0.15 - 0.35$ for $p_T = 1$ TeV,

3. transverse momentum resolution after matching with central detector for $0 \leq |\eta| \leq 2 : \frac{\Delta p_T}{p_T} = 0.005 - 0.01$ for $p_T = 10$ GeV, $0.015 - 0.05$ for $p_T = 100$ GeV and $0.05 - 0.2$ for $p_T = 1$ TeV,

4. charge assignment: correct at 99 percent confidence level up to $p_T = 7$ TeV for the full η coverage,

5. muon trigger: precise muon chambers and fast dedicated detectors provide a trigger with p_T thresholds from a few GeV up to 100 GeV.

Trigger. For the nominal LHC design luminosity 10^{34} $\mathrm{cm}^{-2}\mathrm{s}^{-1}$, an average of 20 inelastic events occur every 25 ns, the beam crossing time interval. The input rate of 10^9 interactions per second must be reduced by a factor of at least 10^7 to 100 Hz, which is the maximum rate that should be achieved for off-line analysis. CMS reduces this rate in two steps. The Level-1 trigger system operates on a subset of the data collected from each LHC crossing. The processing is dead timeless and the decision to collect the full set of data relating to a given crossing is taken after a fixed latency of 3 μs. The maximum event rate which can be accepted by the Level-2 trigger, which again considers a subset of data, is 100 kHz. The Level-1 trigger system comprises the front-end electronics which generates trigger primitives at the detector and the Level-1 processing logic in the electronic barracks, interconnected electrically and optically. The Level-2 trigger

is provided by an online processor farm. After a Level-2 positive decision, the remainder of the full crossing data is requested for further processing by this farm for the final (Level-3) decision.

The benchmarks for the trigger selection correspond to the final states which are not interesting in their own right, but typical of final states expected in new physics processes. They correspond to inclusive triggers that must be highly efficient for new physics signatures. The benchmarks are:

1) electrons from inclusive W bosons,

2) muons from inclusive W bosons,

3) jets at high p_t,

4) high-p_t photons,

5) missing E_T,

6) low-p_T multi-leptons (for b-physics).

8.2. ATLAS Detector [68]. The design of the ATLAS detector is similar to the CMS detector. It also consists of inner detector (tracker), electromagnetic calorimeter, hadron calorimeter, muon spectrometer and trigger. Here we briefly describe the main parameters of the ATLAS subdetectors. A schematic view of the ATLAS detector is shown in Fig. 18.

Inner Detector. The main parameters of the ATLAS inner detector at high-luminosity running are:

1. tracking coverage over the pseudorapidity range $|\eta| \leq 2.5$,

2. momentum resolution of $\frac{\Delta p_T}{p_T} \leq 0.3$ at $p_T = 500$ GeV for $|\eta| \leq 2$ and no worse than 50 percent for $|\eta| = 2.5$,

3. polar-angle resolution of ≤ 2 mrad,

4. tracking efficiency of $\geq 95\%$ over the full coverage for isolated tracks with $p_T \geq 5$ GeV, with fake-track rates less than 1% of signal rates,

5. tracking efficiency of $\geq 90\,\%$ for all tracks with $p_T > 1$ GeV in a cone $\Delta R < 0.25$ around high-p_T isolated track candidates, with less than $10\,\%$ of such tracks being fakes; here, ΔR is defined as the separation of the particles in pseudorapidity-azimuth space,

6. electron-finding efficiency (integrated over all p_T, and including the trigger efficiency) of $> 90\,\%$ for a second electron with $p_T > 0.5$ GeV near a high-p_T candidate, in order to suppress photon-conversion and Dalitz-decay backgrounds,

7. high-p_T electron identification efficiency above $90\,\%$ both in the trigger and in the full reconstruction, including the effects of bremsstrahlung in the tracker material,

8. combined efficiency of the calorimeter and inner detector in excess of $85\,\%$ for finding photons in the $p_T \sim 60$ GeV, with an electron rejection factor > 500 and with an isolated π^0 rejection factor > 3,

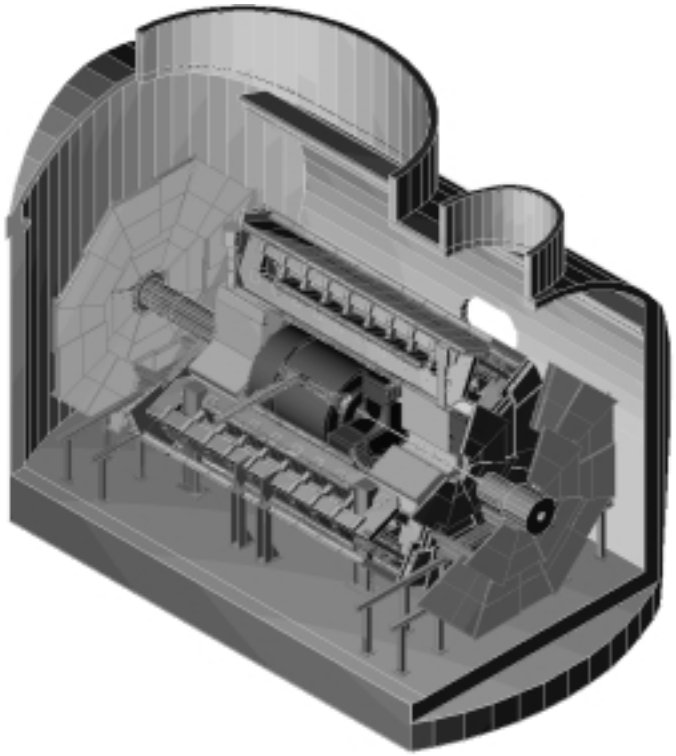

Fig. 18. Three-dimensional view of the ATLAS detector

9. tagging of b jets with an efficiency $\geq 30\,\%$ at the highest luminosity, with a rejection ≥ 10 against non b-hadronic jets,

10. measurement of the z coordinate of primary vertices with at least four charged tracks to better than $1\ \mathrm{mm}$,

11. provision of LVL2 track trigger to select isolated tracks with $p_T > > 20\ \mathrm{GeV}$ with an efficiency $> 90\,\%$ and a fake track rate of $< 10\,\%$, in a cone of $\Delta R < 0.25$ around high-E_T e.m. calorimeter clusters.

For initial lower-luminosity running the additional important parameters are:

1. tagging of b jets with an efficiency above $30\,\%$, with a rejection > 50 against non b-hadronic jets,

2. the ability to reconstruct secondary vertices from b and τ decays and charged tracks from primary vertices and from secondary decay vertices of short-lived particles with $\geq 95\,\%$ efficiency for $p_T \geq 0.5\ \mathrm{GeV}$ over the full coverage,

3. reconstruction and identification of electrons with $p_T > 1\ \mathrm{GeV}$ with an efficiency $> 70\,\%$.

ECAL. The energy resolution is of $\frac{\Delta E}{E} = \frac{0.1}{\sqrt{E}} \oplus 0.007$ for $|\eta| \leq 2.5$. Diphoton mass resolution is estimated to be 1.4 GeV for Higgs boson mass $m_h = 100$ GeV for $L = 10^{34}$ cm^{-2}s^{-1} (for CMS the diphoton mass resolution is 775 MeV).

HCAL. Jet energy resolution is of $\frac{\Delta E}{E} = \frac{0.5}{\sqrt{E}} \oplus 0.03$ for jets and a segmentation of $\Delta\eta \times \Delta\Phi = 0.1 \times 0.1$ for $|\eta| \leq 3$ and $\frac{\Delta E}{E} = \frac{1}{\sqrt{E}} \oplus 0.1$ and a segmentation of $\Delta\eta \times \Delta\Phi = 0.1 \times 0.1$ for very forward calorimeter $3 \leq |\eta| \leq 5$.

Muon Spectrometer. The muon momentum resolution is of $\frac{\Delta p_T}{p_T} = 0.02 (p_T = = 20$ GeV), $\frac{\Delta p_T}{p_T} = 0.02 (p_T = 100$ GeV), $\frac{\Delta p_T}{p_T} = 0.08 (p_T = 1$ TeV) for $|\eta| \leq 3$.

Trigger. The ATLAS trigger is organised in three trigger levels (LVL1, LVL2, LVL3). At LVL1, special-purpose processors act on reduced-granularity data from a subset of the detectors. The LVL2 trigger uses full-granularity, full-precision data from most of the detectors, but examines only regions of the detector identified by LVL1 as containing interesting information. At LVL3, the full event data are used to make the final selection of events to be recorded for off-line analysis. The LVL1 trigger accepts data at the full LHC bunch-crossing rate of 40 MHz (every 25 ns) and reduces them to 100 kHz. The LVL2 trigger reduces the rate from up to 100 kHz after LVL1 to about 1 kHz. After an event is accepted by the LVL2 trigger, the full data are sent to the LVL3 processors which must achieve a data-storage rate of $10 - 100$ MB/s by reducing the event rate and/or the event size.

9. SEARCH FOR STANDARD HIGGS BOSON AT THE LHC

In this section we give mainly the results of the simulations on the search for Higgs boson at CMS detector [67, 70–86]. We don't give the review of the corresponding ATLAS simulations [68,87–96] on the Higgs boson search because the results in terms of the significances coincide up to 30%. However sometimes we compare the CMS and ATLAS Higgs boson discovery potentials.

9.1. The Search for $h \to \gamma\gamma$. One of the most important reactions for the search for Higgs boson at LHC is

$$pp \to (h \to \gamma\gamma) + \dots , \tag{103}$$

which is the most promising one for the search for Higgs boson in the most interesting region 100 GeV $\leq m_h \leq 140$ GeV.

The key features that enable CMS detector to obtain clear two-photon mass peaks, significantly above background throughout the intermediate mass range, are:

i. an electromagnetic calorimeter with an excellent energy resolution (this requires calibration to high precision, which in turn requires a good inner tracking system),

ii. a large acceptance (the precision electromagnetic calorimetry extends to $|\eta| = 2.5$), adequate neutral pion rejection and (at high luminosity) a good measurement of photon direction. This requires fine lateral segmentation and a preshower detector,

iii. use of powerful inner tracking system for isolation cuts.

The cross section (including factor $K = 1.5$) times branching has been estimated to be $\sigma Br(h \to \gamma\gamma) = 76$ fb (68 fb) for $m_h = 110(130)$ GeV, the uncertainty in the cross section calculation is (10–30) percent. The imposition of cuts ($|\eta| \leq 2.5$, $p_T^{\gamma_1} \geq 40$ GeV, $p_T^{\gamma_2} \geq 25$ GeV) allows one to decrease the background in a reasonable magnitude. The jet background is reduced by imposing an isolation cut, which also reduces the bremsstrahlung background. Photon is defined to be isolated if there is no charged track or electromagnetic shower with a momentum greater than 2.5 GeV within a region $\Delta R \leq 0.3$ around it. The photons from the decay of π^0 of the relevant transverse momenta are separated in the calorimeter by a lateral distance of the order of 1 cm. An efficiency of $64\,\%$ was assumed for reconstruction of each photon (i.e., $41\,\%$ per event). The crystal calorimeter was assumed to have an energy resolution $\Delta E/E = 0.02/\sqrt{E} \oplus 0.005 \oplus 0.2/E$ in the barrel and $\Delta E/E = 0.05/\sqrt{E} \oplus$ $\oplus 0.005 \oplus 0.2/E$ in the endcap, where there is a preshower detector. At high luminosity, a barrel preshower detector covers $|\eta| < 1.1$, resulting in a resolution $\Delta E/E = 0.05/\sqrt{E} \oplus 0.005 \oplus 0.2/E$ and an ability to measure the photon direction with resolution $\Delta\alpha = 40\ \mathrm{mrad}/\sqrt{E}$ in this region.

The background to the $h \to \gamma\gamma$ may be divided into 3 categories:

1. Prompt diphoton production from quark annihilation and gluon fusion diagrams — irreducible background.

2. Prompt diphoton production from bremsstrahlung from the outgoing quark line in the QCD Compton diagram.

3. Background from jets, where an electromagnetic energy deposit originates from the decay of neutral hadrons in a jet from 1 jet + 1 prompt photon.

The signal significance $\sigma = \frac{N_S}{\sqrt{N_B}}$ is estimated to be $6.6\sigma(9\sigma)$ for $m_h = 110(130)$ GeV and for low luminosity $L_{\mathrm{low},t} = 3 \cdot 10^4\ \mathrm{pb}^{-1}$ and $10\sigma(13\sigma)$ for $m_h = 110(130)$ GeV and for high luminosity $L_{\mathrm{high},t} = 10^5\ \mathrm{pb}^{-1}$. The general conclusion is that at 5σ level it would be possible to discover Higgs boson*

*It should be noted that more correct definition of the significance in future experiments when we know only the average number of signal N_S and background N_B events is $S = \sqrt{N_S + N_B} - \sqrt{N_B}$ [97]. More appropriate characteristic for future experiments is the probability of the discovery, i.e. the probability that future experiment will measure the number of events N_{ev} such that the probability that standard physics reproduces N_{ev} is less than $5.7 \cdot 10^{-7}$ (5σ). For instance, for the standard Higgs boson search with $m_h = 110$ GeV and for $L = 3 \cdot 10^4\ \mathrm{pb}^{-1}(2 \cdot 10^4\ \mathrm{pb}^{-1})$ the standard significance is 6.6(5.4). At the language of the probabilities it means [97] that the CMS will discover at $\geq 5\sigma$ the Higgs boson with the probability 96(73) percent.

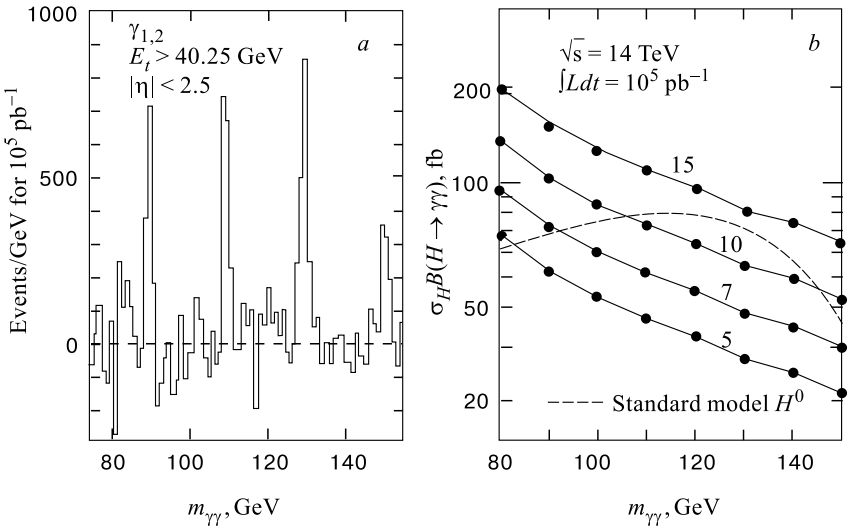

Fig. 19. (*a*) Background-subtracted 2γ mass plot for $10^5 \mathrm{pb}^{-1}$ with signals at $m_h = 90,\ 110,\ 130$ and 150 GeV in $PbWO_4$ calorimeter (CMS). (*b*) Signal significance contours for $10^5 \mathrm{pb}^{-1}$ taken at high luminosity (CMS) ($H \equiv h$)

for $95\ \mathrm{GeV} \leq m_h \leq 145\ \mathrm{GeV}$ at low luminosity and at high luminosity the corresponding Higgs boson mass discovery interval is $85\ \mathrm{GeV} \leq m_h \leq 150\ \mathrm{GeV}$ (see Fig. 19).

Comparison of the ATLAS and CMS discovery potential for the $h \to \gamma\gamma$ channel has been made in Ref. 89. The ratio between the CMS and ATLAS significances is determined by the formula

$$\frac{S_{\mathrm{CMS}}}{S_{\mathrm{ATLAS}}} \approx \sqrt{\frac{\Delta_m(\mathrm{ATLAS})}{\Delta_m(\mathrm{CMS})}} \times \frac{\epsilon_\gamma(\mathrm{CMS})}{\epsilon_\gamma(\mathrm{ATLAS})}\,, \tag{104}$$

where Δ_m, the diphoton mass resolution, and ϵ_γ, the total photon efficiency (trigger, identification, reconstruction), are detector dependent. In ATLAS and CMS the photon identification efficiencies are 80% [68] and 71% [67] correspondingly. However the diphoton mass resolution is better in CMS. According to the Technical Proposals for $m_h = 110$ GeV the diphoton mass resolutions are:

$$\Delta_m(\mathrm{CMS}) = 0.54\ \mathrm{GeV},\ \Delta_m(\mathrm{ATLAS}) = 1.25\ \mathrm{GeV}\ (\text{low luminosity}),$$

$$\Delta_m(\mathrm{CMS}) = 0.87\ \mathrm{GeV},\ \Delta_m(\mathrm{ATLAS}) = 1.43\ \mathrm{GeV}\ (\text{high luminosity}).$$

The main conclusion of Ref. 89 is that the discovery potential of the CMS (in terms of σ) is $10\,\%$ and $30\,\%$ better than ATLAS at high- and low-luminosity stages correspondingly (for $m_h = 110$ GeV).

9.2. Search for $h \to \gamma\gamma$ in Association with High-E_T Jets. The idea to look for Higgs boson signal associated with a high-p_t jet in the final state was considered in Ref. 82, where the matrix elements of signal subprocesses $gg \to g + h$, $gq \to q + h$ and $q\bar{q}g + h$ have been calculated analytically in the leading order α_s^3. One kind of reducible background comes from the reactions $qg \to \gamma + g + q$, $gg \to \gamma + q + \bar{q}$, $qq^{'} \to \gamma + q(g) + q^{'}(g)$ in the cases when the final gluon or quark produces an energetic photon without further jet generation. Other kind of reducible background comes from the subprocesses $qg \to \gamma + q, q\bar{q}\gamma + g$ when the second photon is produced during the quark or gluon fragmentation but this jet is still detected. Third kind of reducible background could come from the pure QCD subprocesses $2 \to 2$ type, when both particles in the final state are gluons and quarks. There is nonzero probability to get two separated and energetic photons from the fragmentating of quarks and gluons. There are possible contributions from the following subprocesses: $gg \to g(q) + g(\bar{q})$, $gq \to g + q$, $qq^{'} \to q(g) + q^{'}(g)$.

The typical set of cuts used to separate signal from background is [82]:

(C1) Two photons are required with $p_t^{\gamma} > 40$ GeV, and $|\eta|_{\gamma} < 2.5$ for each photon.

(C2) Photons are isolated from each other by $\Delta R(\gamma_1, \gamma_2) > 0.3$.

(C3) Jet has high transverse energy $E_t^{\text{jet}} > 40$ GeV and is centrally produced, $|\eta_{\text{jet}}| < 2.4$.

(C4) Jet is isolated from the photons by $\Delta R(\text{jet}, \gamma_1) > 0.3$ and $\Delta R(\text{jet}, \gamma 2) > 0.3$.

For the Higgs boson mass $100\ \text{GeV} \le M_h \le 150\ \text{GeV}$ and for an integrated luminosity $10\ \text{fb}^{-1}$ this channel has dozens of signal events with a number of background events only by a factor of 2–3 higher [82]. The significance $N_S/\sqrt{N_B} \sim 4.0; 5.3$ and 4.1 for $M_h = 100, 120$ and 140 GeV respectively, indicating good prospects for discovery of the light Higgs boson at low LHC luminosity. These results also imply that at high luminosity phase with year luminosity of $10^5\ \text{pb}^{-1}$ LHC will give hundred of events with high p_t associated with hard jet with the signal significance ~ 15.

Note that recent study [92] of the signature $\gamma\gamma +$ jets for ATLAS detector confirms the main results of Ref. 82.

The possibility of searching for $h \to \gamma\gamma$ with ≥ 2 large-E_T jet also allows one to improve $\text{signal}/\text{background}$ ratio. There are several sources of such Higgs + jet events. One is the next-to-leading order corrections to $gg \to h$ with hard gluons. Others are the associated production of $\bar{t}th, Wh, Zh$ and the WW and Zh fusion mechanisms.

The cuts that provide optimal sensitivity are [73]:

i. Two isolated photons are required, with $p_t^{\gamma_1} \ge 40$ GeV and $p_t^{\gamma_2} \ge 60$ GeV, $|\eta| \le 2.5$ and $p_t^{\gamma\gamma} \ge 50$ GeV.

ii. Number of jets ≥ 2, $E_t^{\rm jet} \geq 40$ GeV for the central jets ($|\eta| \leq 2.4$) and $E^{\rm jet} \geq 800$ GeV for the forward ones ($2.4 \leq |\eta| \leq 4.6$).

iii. Photons are isolated with no charged or neutral particles with $p_t \geq 2$ GeV within a cone $\Delta R \leq 0.3$ around each photon's direction.

iiii. γ-jet isolation $\Delta R(\gamma, {\rm jet}) > 1.5$ (to suppress the bremsstrahlung contribution).

The calculations give encouraging results, namely for $L_{{\rm high},t} = 1.6 \cdot 10^5$ pb^{-1} it would be possible to discover the Higgs boson for 70 GeV $\leq m_h \leq$ 150 GeV with $\geq 7\sigma$ signal significance. Note that the background is not only much smaller in magnitude than in the inclusive $h \to \gamma\gamma$ search, but it is also peaked at higher masses, away from the most difficult region $m(\gamma\gamma) \leq 90$ GeV.

9.3. $h \to W^+W^- \to l^+\nu l^-\nu$ **Signature.** Recently it has been shown [83] that the previously ignored signature $pp \to h \to W^+W^- \to l^+\nu l^{'-}\bar{\nu}'$ provides the Higgs boson discovery for the Higgs boson mass region between 155 GeV and 180 GeV at the LHC. The proposed signature does not require extraordinary detector performance and only requires a relatively low integrated luminosity of about 5 fb^{-1}.

The main background production reactions are

$$pp \to (W^+W^-, W^\pm Z^0, t\bar{t}, W^\pm t(b) + ...). \tag{105}$$

The most important selection criteria for the enhancement of the signal over the background are the following [83]:

1. Events which contain two isolated high-p_t charged leptons, electrons or muons, which are inconsistent with Z decays are selected. Both leptons should have a pseudorapidity $|\eta|$ of less than 2.4 and their p_t should be larger than 25 GeV and 10 GeV respectively. The dilepton mass should be larger than 10 GeV and more than 5 GeV different from Z boson mass if the event consists of e^+e^- or $\mu^+\mu^-$ pairs.

2. Background from $t\bar{t} \to bW^+\bar{b}W^-$ and $gb \to Wtb \to WbW(b)$ is reduced by vetoing events which contain jets with p_t of more than 20 GeV and $|\eta| < 3$.

3. Signal events from gluon-gluon scattering are more central than the W^+W^- background from $q\bar{q}$ scattering. This criterium is essentially independent of the mass. Therefore it is required that the polar angle of the reconstructed dilepton momentum vector, with respect to the beam direction, is larger than 30 degrees and that the absolute value of the pseudorapidity difference of the leptons is smaller than 1.25. As a result both leptons are found essentially within the barrel region of the experiments with $|\eta| < 1.5$.

4. The W^+W^- spin correlations and the $V - A$ structure of the W decays result in a distinctive signature for W^+W^- pairs produced in Higgs boson decays. For Higgs boson mass close to $2 \times M_W$ the $W^\pm$ boost is small and the

opening angle between the two charged leptons in the plane transverse to the beam direction is small.

The results of the analysis [83] demonstrate that this signature provides not only the Higgs boson discovery channel for a mass range between $(155-180)$ GeV with $S/B \geq 0.35$ but also helps to establish a LHC Higgs boson signal for masses between $(120-500)$ GeV. Recent simulations study [84] based on PYTHIA to generate events and CMSCIM calorimeter simulation for the jet veto confirm qualitatively the results of Ref. 83. Numerically they give for $m_h = 130$ GeV $30\,\%$ lower efficiencies for the signal and DY background and about a factor 2 higher overall efficiency for $t\bar{t}$ background [84].

Note that in Ref. 98 the signature $h \to W^{(*)}W^{(*)} \to e^{\pm}\mu^{\mp}p_T^{\rm mis}$ in weak boson fusion mechanism with forward jet tagging has been investigated*. The main conclusion of Ref. 98 is that the use of this signature allows one to detect Higgs boson in the $(130-200)$ GeV range with a much better signal to background ratio than inclusive signature $h \to e^{\pm}\mu^{\mp}p_T^{\rm mis}$.

9.4. $h \to ZZ^*(ZZ) \to 4$ **Leptons.** $m_h < 2m_Z$ **Region**. The channel $h \to ZZ^* \to 4\,l$ is the most promising one to observe Higgs boson in the mass range 130 GeV $-$ 180 GeV. Below $2M_Z$ the event rate is small and the background reduction more difficult, as one of the Z is off-mass shell. In this mass region the width of the Higgs boson is small ($\Gamma_h < 1$ GeV), and the observed width is entirely determined by the instrumental mass resolution. The significance of the signal is proportional to the four-lepton mass resolution ($S = N_S/\sqrt{N_B}$) and $N_B \sim \sigma_{4l}$, so the lepton energy/momentum resolution is of decisive importance**.

In the $m_h < 2M_Z$ mass region, the main backgrounds are from $t\bar{t}$, $Zb\bar{b}$ and ZZ^*. The ZZ^* background is irreducible and peaks sharply near the ZZ threshold. The $Zb\bar{b}$ background cannot be reduced by a Z-mass cut, but it can be suppressed by lepton isolation. The $t\bar{t}$ background can be reduced by a Z-mass cut and by isolation cuts. The standard event cuts in CMS were chosen the following [67]: one electron with $p_t > 20$ GeV; one with $p_t > 15$ GeV, and the remaining two electrons with $p_t > 10$ GeV, all within $|\eta| < 2.5$. For muons, the corresponding p_t cuts are 20, 10 and 5 GeV in the rapidity range $|\eta| < 2.4$. For $m_h = 130$ GeV the overall (kinematic and geometrical) acceptance for the four-

*Other very interesting signature for the standard Higgs boson detection is $h \to \tau\tau$ in weak boson fusion. Results of recent paper [99] give some evidence that it would be possible to detect standard Higgs boson in the mass range $120-140$ GeV using this signature.

**Typical Higgs boson mass resolutions in this mass range are: $\sigma_{4\mu} \approx 1$ GeV, $\sigma_{4e} \approx 1.5$ GeV (CMS) [67] and $\sigma_{4\mu} \approx 1.6$ GeV, $\sigma_{4e} \approx 1.6$ GeV (ATLAS) [68]. The comparison of the CMS and ATLAS discovery potentials with $h \to ZZ^* \to 4$ leptons based on the analyses presented in the two Technical Proposals has been performed in [88]. The main conclusion of the Ref. 88 is that in terms of significances ATLAS and CMS discovery potentials coincide up to 30%.

electron channel is $22\,\%$ and for the four-muon channel $42\,\%$. For $m_h = 170$ GeV these acceptances increase to $38\,\%$ and $48\,\%$ respectively. To select $h \to ZZ^*$ events and suppress the large $t\bar{t}$ background, one of the e^+e^- or $\mu^+\mu^-$ pairs was assumed to be within $\pm 2\sigma_Z$ of the Z mass. There is a fraction of events where both Z are off-shell. This effect results in a $24\,\%$ loss for $m_h = 130$ GeV, decreasing to $12\,\%$ for $m_h = 170$ GeV. The M_Z cut reduces $t\bar{t}$ background by a factor of 11 in the $Z \to \mu^+\mu^-$ channel and by a factor of 5 in the $Z \to e^+e^-$ channel. For two softer leptons, $M(ll) > 12$ GeV is also required. One can say that for the region 130 GeV $\leq m_h \leq$ 180 GeV and for $L_{\mathrm{high},t} = 10^5$ pb^{-1} CMS will discover the Higgs boson with $\geq 5\sigma$ signal significance (see Fig. 20) except narrow mass region around 170 GeV where $\sigma \times Br$ has a minimum due to the opening of the $h \to WW$ channel and drop of the $h \to ZZ^*$ branching ratio just below the ZZ threshold. Note that the imposition of the additional cut on the mass of the second (lighter) lepton pair to $m_{34} < 76$ GeV leads to a considerable signal improvement in this critical region. At low luminosity $L = 2 \cdot 10^4$ pb^{-1} Higgs boson can be discovered at CMS in the mass range $m_h = (130 - 150)$ GeV.

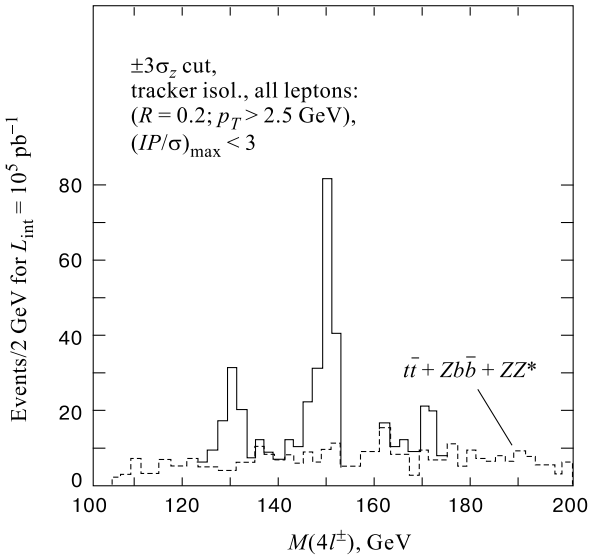

Fig. 20. The four-lepton mass distributions for $h \to ZZ^* \to 4l^{\pm}$ in CMS, superimposed on the total background, for $m_h = 130,\ 150$ and 170 GeV with $10^5 \mathrm{pb}^{-1}$ ($H \equiv h$)

$h \to ZZ \to 4l$. For 180 GeV $\leq m_h \leq$ 800 GeV, this signature is considered to be the most reliable one for the Higgs boson discovery at LHC, since the expected signal rates are large and the background is small. The main background

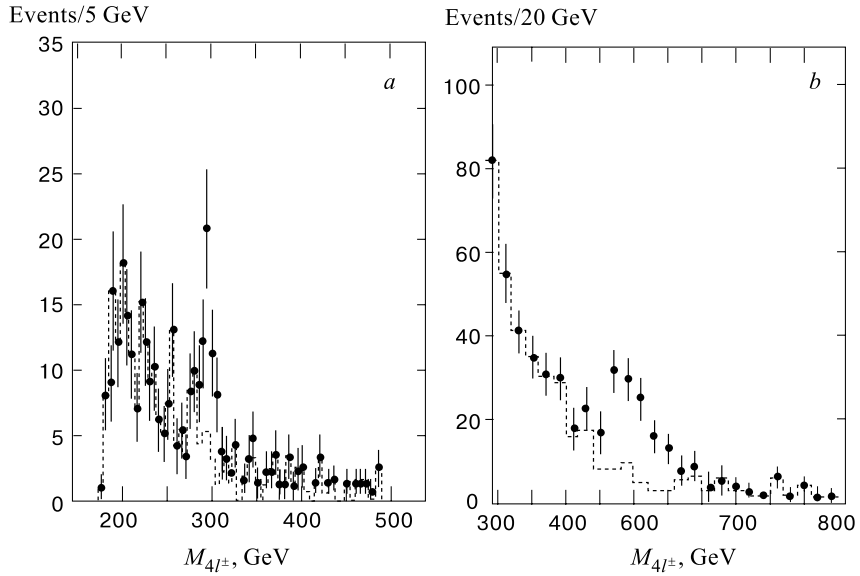

Fig. 21. The four-lepton mass distributions for $h \to ZZ \to 4l^\pm$ in CMS, superimposed on the ZZ continuum background, for $m_h = 300$ GeV with $2 \cdot 10^4 \mathrm{pb}^{-1}$ (*a*) and for $m_h = 500$ GeV with $10^5 \mathrm{pb}^{-1}$ (*b*); $\sqrt{s} = 14$ TeV ($H \equiv h$)

to the $h \to ZZ \to 4l^\pm$ process is the irreducible ZZ production from $q\bar{q} \to ZZ$ and $gg \to ZZ$. The $t\bar{t}$ and $Zb\bar{b}$ backgrounds are small and reducible by a Z-mass cut. The typical cuts are the following [76, 77]:

1. One electron with $p_T > 20$ GeV, one with $p_T > 15$ GeV, and the remaining two electrons with $p_T > 10$ GeV, all within $|\eta| < 2.5$.

2. For muons the corresponding p_T cuts are 20, 10 and 5 GeV, and the rapidity coverage is $|\eta| < 2.4$.

3. To avoid any residual $t\bar{t}$ background a cut on the Z mass by $m_{l^+l^-} = m_Z \pm 4\sigma_Z$, with $\sigma_Z = 3$ GeV is used.

The use of the above determined cuts allows one to detect the Higgs boson at $\geq 5\sigma$ level up to ≈ 400 GeV at 10^4 pb^{-1} and up to $m_h \approx 650$ GeV at 10^5 pb^{-1} [77] (see Fig. 21). As it has been demonstrated in Ref. 77 the imposition of the additional cut $p_T^{Z_1} + p_T^{Z_2} > m_{ZZ}/1.4$ allows one to extend the CMS discovery potential up to 650 GeV($3 \cdot 10^4$ pb^{-1}), 750 GeV(10^5 pb^{-1}), 850 GeV($3 \cdot 10^5$ pb^{-1}).

Similar results have been obtained for ATLAS [91].

9.5. The Use of the Signature $pp \to \gamma\gamma +$ Lepton. The $Wh \to l\gamma\gamma + X$ and $\bar{t}th \to l\gamma\gamma + X$ final states are other promising signature for the Higgs boson search. The production cross section is smaller than the inclusive $h \to \gamma\gamma$ by

a factor of ≈ 30. However the isolated hard lepton from the W and t decays allows one to obtain a strong background reduction and to indicate the primary vertex at any luminosity.

Typical choice of cuts is the following [67, 72]:

1. $p_t^{\gamma_1} > 40$ GeV, $p_t^{\gamma_2} > 20$ GeV, transverse momentum cuts for photons,

2. $p_t^l > 20$ GeV, transverse momentum cuts for electron (or muon),

3. $|\eta_{\gamma_1,\gamma_2}| < 2.4, |\eta_l| < 2.4$, rapidity cuts for both photons and electron (or muon),

4. $\Delta R(\gamma_1, \gamma_2) > 0.3$, $\Delta R(\gamma, l) > 0.3$, isolation cuts for photon or photon-lepton pair.

Here $\Delta R = \sqrt{\delta\phi^2 + \delta y^2}$ is the separation between two particles in the ϕ–y plane. The main background comes from the reactions $pp \to \gamma\gamma + t\bar{t}$, $pp \to \gamma q(\bar{q} + e^{\pm}\nu)$, $pp \to \gamma g + e^{\pm}\nu$ with a gluon jet misidentified as a photon, $pp \to \gamma + e^+e^-$ with an electron misidentified as a photon, $pp \to \gamma\gamma b\bar{b}$ with a b quark misidentified as an electron.

The main conclusion is that for an integrated luminosity 165fb^{-1} in both channels $pp \to Wh$ and $pp \to t\bar{t}h$ in the two-photon invariant mass interval $M_h - 1$ GeV $\leq M_{\gamma\gamma} \leq M_h + 1$ GeV there are ~ 100 signal events for $M_h = 120$ GeV and ~ 20 irreducible background events if the photon transverse momentum cuts are 20 GeV. If the photon transverse momentum cuts are taken to be 40 GeV there are ~ 50 signal events and $1 - 2$ background events. Higgs peak can be observed practically free from the background. However in the low luminosity regime the reaction $pp \to \gamma\gamma + \text{lepton}$ is able to produce only $4 - 5$ clean signal events. So only in the high luminosity phase it allows one to make an important cross-checking if the Higgs signal has shown up before in $pp \to h + ... \to \gamma\gamma + ...$ classical signature.

9.6. The Use of Channels $h \to WW \to ll\nu\nu$, $h \to WW \to l\nu jj$ and $h \to ZZ \to lljj$. The channel $h \to ll\nu\nu$ has a six times larger branching than $h \to 4l^{\pm}$. The main background comes from ZZ, ZW, $t\bar{t}$ and $Z + \text{jets}$. The chosen cuts are the following [67]:

1. $E_t^{\text{miss}} \geq 100$ GeV.

2. Two isolated leptons are required, with $p_t \geq 20$ GeV, $|\eta| \leq 1.8$ and $p_t^{ll} \geq 60$ GeV.

3. $|M_Z - M_{ll}| \leq 6$ GeV.

4. No other isolated leptons with $p_t \geq 6$ GeV.

5. No central jets with $E_t \geq 150$ GeV.

6. No jets back-to-back with leptons (cosine of the angle between the momentum of the lepton pair and sum of the momenta of the jets is ≥ -0.8).

7. E_t^{miss} vector back-to-back with the lepton pair (cosine of the angle in the transverse plane between the two-lepton momentum and the missing transverse momentum ≤ 0.8).

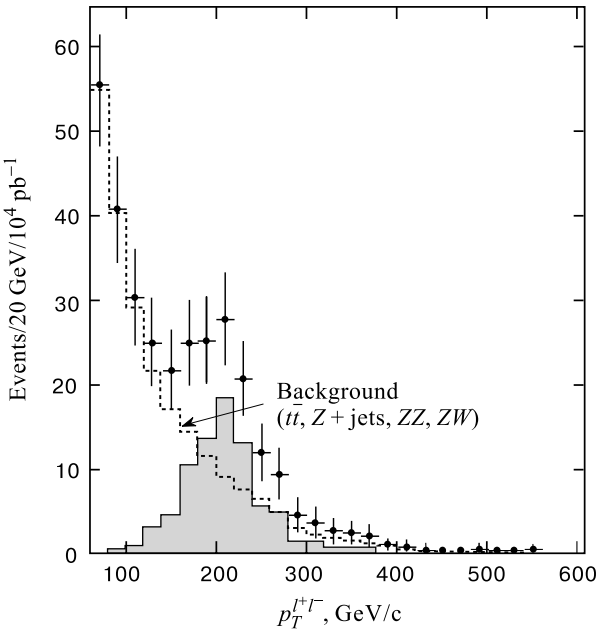

Fig. 22. $h \to l^+l^-\nu\nu$ signal for $m_h = 500$ GeV with $10^4 \mathrm{pb}^{-1}$ in CMS ($H \equiv h$)

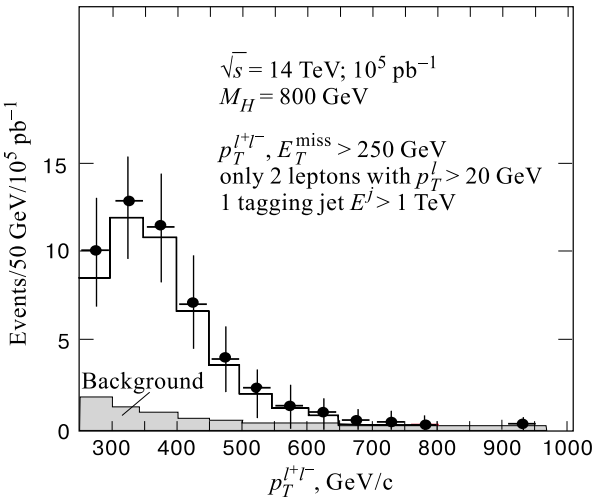

Fig. 23. $h \to l^+l^-\nu\nu$ signal for $m_h = 800$ GeV with $10^5 \mathrm{pb}^{-1}$ in CMS. One tagged jet with $E > 1$ TeV is assumed ($H \equiv h$)

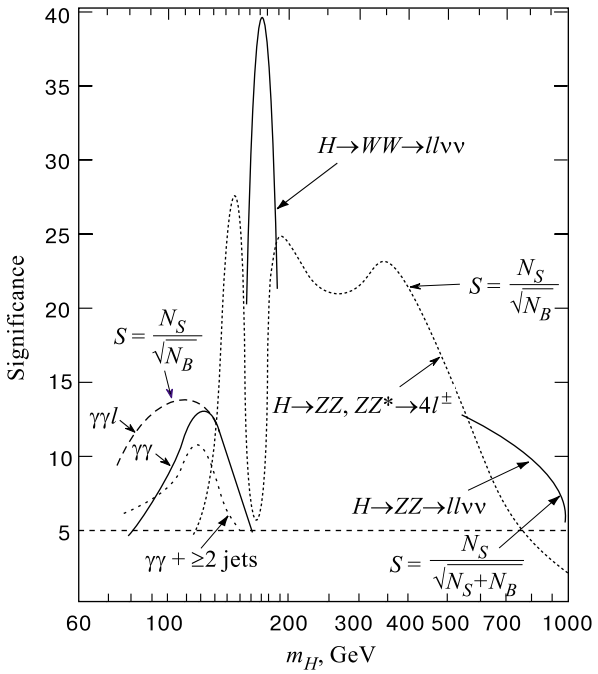

Fig. 24. Expected observability of the Standard Model Higgs as a function on m_H in CMS with $10^5 \mathrm{pb}^{-1}$ (Ref. 79) ($H \equiv h$)

The conclusion [67, 86] is that using this mode it would be possible to discover Higgs boson in the interval $400\ \mathrm{GeV} \leq m_h \leq (800 - 900)\ \mathrm{GeV}$ (see Figs. 22, 23).

The channels $h \to WW \to l\nu jj$ and $h \to ZZ \to lljj$ are important in the $m_h \approx 1$ TeV mass range, where the large $W, Z \to q\bar{q}$ branching ratios must be used. Also high lepton pairs with $m_{ll} \approx M_Z$ for $h \to ZZ$ or a high-p_t lepton pair plus large E_t^{miss} for $h \to WW$ must be used. In addition, two hard jets from the hadronic decays of Z/W with $m_{jj} \approx M_{Z/W}$ are required. The backgrounds are: $Z + \mathrm{jets}$, ZW, WW, $t\bar{t}$, WW, WZ. For $m_h \approx 1$ TeV the Higgs boson is very broad ($\Gamma_h \approx 0.5$ TeV and WW/ZZ fusion mechanism represents about 50 percent of the total production cross section), therefore forward-region signature is essential. The appropriate cuts are the following:

i. $E_t^{\mathrm{miss}} \geq 150$ GeV, $p_t^l \geq 150$ GeV, $p_t^W \geq 300$ GeV for $h \to WW$, or $p_t^l \geq 50$ GeV, $p_t^Z \geq 50$ GeV, $p_t^Z \geq 150$ GeV, $|m_Z - m_{ll}| \leq 10$ GeV for $h \to ZZ$.

ii. $|m_{jj} - m_{W/Z}| \leq 15$ GeV for the central jet pair.

iii. $E_t^{\mathrm{jet}} \geq 10$ GeV, $E^{\mathrm{jet}} \geq 400$ GeV, $|\eta| \geq 2.4$ for the two forward tagging jets.

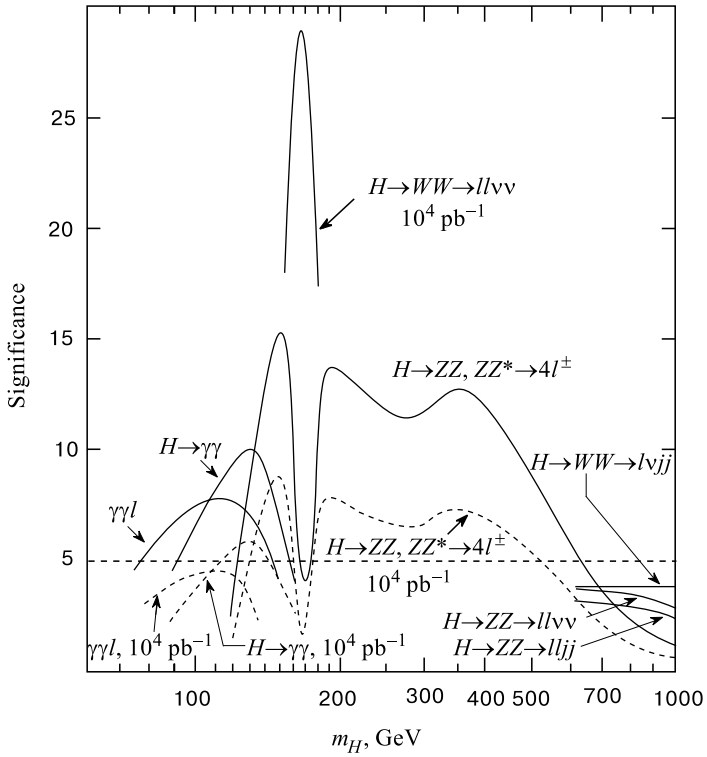

Fig. 25. Expected observability of the Standard Model Higgs as a function on m_H in CMS with $3 \cdot 10^4 \mathrm{pb}^{-1}$ and with $10^4 \mathrm{pb}^{-1}$ (Ref. 79) ($H \equiv h$)

The main conclusion [67, 78] is that the use of the reactions $h \to WW \to$ $\to l\nu jj$ and $h \to ZZ \to lljj$ allows one to discover the heavy Higgs boson with a mass up to 1 TeV for $L_{\mathrm{high},t} = 10^5\ \mathrm{pb}^{-1}$.

9.7. Summary. The most reliable signatures for the search for the Higgs boson at LHC are the following:

1. $h \to \gamma\gamma$ or $h \to \gamma\gamma +$ jets.
2. $h \to ZZ^*, ZZ \to 4\ l^{\pm}$.
3. $h \to W^+W^- \to l^+\nu l^-\bar{\nu}$.
4. $h \to ZZ, WW \to ll\nu\nu,\ lljj,\ l\nu jj$.

Figures 24, 25 show the expected CMS discovery potential of the standard Higgs boson as a function of m_h for integrated luminosities of $10^5\ \mathrm{pb}^{-1}$ and $3 \cdot 10^4\ \mathrm{pb}^{-1}$. For $L = 10^5\ \mathrm{pb}^{-1}$ CMS is able to discover the Higgs boson at $\geq 5\sigma$ level for the entire mass region (95 GeV–1 TeV). For low luminosity stage with $L = 3 \cdot 10^5\ \mathrm{pb}^{-1}$ CMS is able to discover Higgs boson with a mass up to ~ 600 GeV.

10. CONCLUSION

There are no doubts that at present the supergoal number one of the experimental high energy physics is the search for the Higgs boson — the last nondiscovered cornerstone of the Standard Model. At present the LEP2 experimental bound on the Higgs boson mass is $m_h \geq 102.6$ GeV. In a year, LEP2 will be able to discover the Higgs boson or to increase a lower bound up to $(105 - 110)$ GeV. LHC is able to discover the Higgs boson with a mass up to 1 TeV and to check its basic properties. The experimental Higgs boson discovery will be triumph of the idea of the renormalizability (in some sense it will be the «experimental proof» of the renormalizabilty of the electroweak interactions) which mathematical cornerstone is the famous Bogoliubov–Parasiuk theorem. At any rate after LHC we will know the basic mechanism (Higgs boson or something more exotic?) of the electroweak symmetry breaking.

We thank our colleagues from INR theoretical department for useful discussions. We are indebted to S.I.Bityukov for his help in preparation of the manuscript. The research described in this publication has been supported by RFFI grants 99-02-16956 and 99-01-00091.

REFERENCES

1. **Bogoliubov N.N., Shirkov D.V.** — Introduction to the Theory of Quantized Fields (3rd ed.), John Wiley Inc., New York, 1980.
2. **Bogoliubov N.N., Parasyuk D.V.** — Dokl. Akad. Nauk SSSR, 1956, v.100, p.429; Acta Mathem., 1957, v.97, p.227.
3. **Bogoliubov N.N. et al.** — General Principles of Quantum Field Theory, Nauka, Moscow, 1987.
4. **Glashow S.L.** — Nucl. Phys., 1961, v.22, p.579;
   Weinberg S. — Phys. Rev. Lett., 1967, v.19, p.1264;
   Salam A. — Elementary Particle Theory (ed. N.Svartholm), Almquist and Wiksells, Stockholm, 1964.
5. **Higgs P.** — Phys. Lett., 1964, v.12, p.132;
   Englert F., Brout R. — Phys. Rev. Lett., 1964, v.13, p.321.
6. **Bogoliubov N.N.** — J. Phys. USSR, 1947, v.11, p.23; Lectures on Quantum Statistics, Mackdonald Technical and Scientific, London, 1970.
7. **Accomando E. et al.** — Phys. Rep., 1998, v.299, p.1.
8. **Barger V. et al.** — Phys. Rep., 1997, v.286, p.1.
9. Reviews and original references can be found in:
   Barbieri R. — Riv. Nuovo Cim., 1988, v.11, p.1;
   Lahanus A.B., Nanopoulos D.V. — Phys. Rep., 1987, v.145, p.1;
   Haber H.E., Lane G.L. — Phys. Rep., 1985, v.117, p.75;
   Nilles H.P. — Phys. Rep., 1984, v.110, p.1.
10. **Okun L.B.** — Leptons and Quarks, North Holland Pub. Comp., 1982.

11. **Ta-Pei Cheng, Ling-Fong-Li** — Gauge Theory of Elementary Particle Physics, Oxford University Press, Oxford, 1984.
12. **Pokorsky S.** — Gauge Field Theories, Cambridge University Press, Cambridge, 1987.
13. **Bailin D., Love A.** — Introduction to Gauge Field Theory, Adam Hilger, Bristol, 1986.
14. **Gunion J.F. et al.** — The Higgs Hunter's Guide, Addison-Wesley Publishing Company, Redwood City, CA, 1990.
15. **Borodulin V.I., Rogalyov R.N., Slabospitsky S.R.** — Compendium of Relations, IHEP Preprint 95-50.
16. **Spira M., Zervas P.M.** — Electroweak Symmetry Breaking and Higgs Physics, CERN-TH/97-379 [hep-ph/9803257].
17. **Spira M.** — QCD Effects in Higgs Physics, CERN-TH/97-68 (hep-ph/9705337), Fortsch.Phys., 1998, v.43, p.203.
18. **Dittmar M.** — Searching for the Higgs and Other Exotic Objects, CMS CR 1999/009; ETHZ-IPP PR-98-10.
19. Review of Particle Physics, The European Physical Journal, 1998, v.C3.
20. **Lee B.W., Quigg C., Thacker C.B.** — Phys. Rev. Lett., 1977, v.38, p.883; Phys. Rev., 1974, v.D10, p.1145.
21. **Dawson S., Willenbrock S.** — Phys. Rev., 1989, v.D40, p.2880.
22. See for instance:
Jersak J. — In: Higgs Particles(s), Proceedings of the Eighth INFN Eloisatron Project Workshop, July 15-26, Erice, Italy, edited by A.Ali, Plenum Press, New York, 1990, p.39.
23. **Cabibbo N. et al.** — Nucl. Phys., 1979, v.B158, p.295;
Lindner M. — Z. Phys., 1986, v.C31, p.295.
24. **Krasnikov N.V.** — Sov. J. Nucl. Phys., 1978, v.28, p.549;
Hung P.Q. — Phys. Rev. Lett., 1979, v.42, p.873;
Politzer H.D., Wolfram S. — Phys. Lett., 1979, v.B82, p.242;
Anselm A.A. — JETP Lett., 1979, v.29, p.590;
Lindner M., Sher M., Zaglauer M. — Phys. Lett., 1989, v.B228, p.139.
25. **Krasnikov N.V., Kreyerhoff G., Rodenberg R.** — Mod. Phys. Lett., 1994, v.A9, p.3663.
26. **Ellis J., Ridolfi G., Zwirner F.** — Phys. Lett., 1991, v.B257, p.83;
Haber H., Hempfling R. — Phys. Rev. Lett., 1991, v.66, p.1815;
Yamada A. — Phys. Lett., 1991, v.B263, p.233;
Barbieri R., Frigeni M., Caravaglis F. — Phys. Lett., 1991, v.B258, p.233;
Chanowski P.M., Pokorski S., Rosick J. — Phys. Lett., 1992, v.B275, p.191.
27. **Krasnikov N.V., Pokorski S.** — Phys. Lett., 1992, v.B288, p.184;
Diaz M.A., Ter Veldhuis T.A., Weiler T.J. — Phys. Rev. Lett., 1995, v.74, p.2876; Phys. Rev., 1996, v.D54, p.5855.
28. **Veltman M.** — Acta Phys. Polon., 1977, v.B8, p.475; See also:
Dittmaier S., Schildknecht D., Weiglein S. — Phys. Lett., 1996, v.B386, p.247.
29. A Combination of Preliminary Electroweak Measurements and Constraints on the Standard Model, the LEP Collaborations, LEPEWWG/98-01, 15 May 1998.
30. **Chanowitz M.S.** — Higgs Boson Mass Constraints from Precision Data and Direct Searches, LBNL-42103(1998)[hep-ph/9807452].
31. **Resnick L., Sundarsean M.K., Watson P.J.S.** — Phys. Rev., 1973, v.D8, p.172;
Ellis J., Gaillard M.K., Nanopoulos D.V. — Nucl. Phys., 1976, v.B106, p.292.

32. **Braaten E., Leveille J.P.** — Phys. Rev., 1980, v.D22, p.715;
Sakai N. — Phys. Rev., 1980, v.D22, p.2220;
Drees M., Hikasa K. — Phys. Rev., 1990, v.D41, p.1547;
Kataev A.L., Kim V.T. — Mod. Phys. Lett., 1994, v.A9, p.1309;
Chetyrkin K.G. — Phys. Lett., 1997, v.B390, p.309.

33. **Cray N. et al.** — Z. Phys., 1990, v.C48, p.673.

34. **Fleischer J., Jegerleher F.** — Phys. Rev., 1981, v.D23, p.2001;
Bardin D.Yu., Vilenski B.M., Khristova P.Kh. — Sov. J. Nucl. Phys., 1991, v.53, p.152;
Dabelstein A., Holik W. — Z. Phys., 1992, v.C53, p.507;
Kniehl B.A. — Nucl. Phys., 1992, v.B376, p.3.
Ghinculov A. — Phys. Lett., 1994, v.B337, p.137; 1995, v.B346, p.426;
Durand L., Kniehl B.A., Riesselmann K. — Phys. Rev., 1995, v.D51, p.5007.

35. **Kniehl B.A., Spira M.** — Z. Phys., 1995, v.C69, p.77;
Kniehl B.A., Spira M. — Nucl. Phys., 1995, v.B443, p.37.

36. **Ghinculov A.** — Nucl. Phys., 1995, v.B455, p.21;
Frink A. et al. — Phys. Rev., 1996, v.D54, p.4548.

37. **Rizzo T.G.** — Phys. Rev., 1980, v.D22, p.389;
Keung W.-Y., Marciano W.J. — Phys. Rev., 1984, v.D30, p.248.

38. **Cahn R.N.** — Rep. Prog. Phys., 1989, v.52, p.389.

39. **Ellis J., Gaillard M.K., Nanopoulos D.V.** — Nucl. Phys., 1976, v.B106, p.292.

40. **Spira M. et al.** — Nucl. Phys., 1995, v.B453, p.17;
Inami T., Kubotta T., Okada Y. — Z. Phys., 1983, v.C18, p.69;
Djouadi A., Spira M., Zervas P.M. — Phys. Lett., 1991, v.B264, p.440.

41. **Chetyrkin K.G., Kniehl B.A., Steinhauser M.** — Phys. Rev. Lett., 1997, v.79, p.353.

42. **Djouadi A., Gambino P.** — Phys. Rev. Lett., 1994, v.D49, p.3499.

43. **Zheng H., Wu D.** — Phys. Rev., 1990, v.D42, p.3760;
Djouadi A. et al. — Phys. Lett., 1991, v.B257, p.187;
Dawson S., Kauffman R.P. — Phys. Rev., 1993, v.D47, p.1264.

44. **Korner J., Melnikov K., Yakovlev O.** — Phys. Rev., 1996, v.D53, p.3737;
Liao Y., Li X. — Phys. Lett., 1997, v.B396, p.225.

45. **Ioffe B.L., Khoze V.A.** — Sov. J. Part. Nucl., 1978, v.9, p.50;
Bjorken J.D. — Proc. Summer Institute on Particle Physics, Report SLAC-198 (1976).

46. See for example:
Altarelli G., Kleiss R., Verzegnassi C., editors. — Physics at LEP, vol.1: Standard Physics, CERN Yellow Report 86-02 (1986).

47. **Blondel A.** — Precision Electroweak Physics at LEP, CERN-PPE/94-133 (1994);
Janot P. — Searching for Higgs Bosons at LEP1 and LEP2, Perspectives on Higgs Physics, World Scientific Publishing Company, ed.K.G.Lane.

48. Report CERN 96-01, vol.1, «Physics at LEP2», edited by G.Altarelli, T.Sjostrand, F.Zwirner and references therein.

49. **Passarino G.** — Nucl. Phys., 1997, v.B488, p.3.

50. L3 Collaboration, Search for the Standard Model Higgs Boson in e^+e^- Interactions at $\sqrt{s} = 189$ GeV, CERN Preprint CERN-EP/99-080 (1999).

51. The Opal Collaboration, Search for Neutral Higgs Bosons in e^+e^- Collisions at $\sqrt{s} \approx 189$ GeV, CERN Preprint CERN-EP/99-096(1999) [hep-ex/9908002].

52. The ALEPH Collaboration, Search for the Neutral Higgs Bosons of the Standard Model and the MSSM in e^+e^- Collisions at $\sqrt{s} = 188.6$ GeV, ALEPH 99-053(CONF 99-029).

53. The DELPHI Collaboration, DELPHI 99-8(CONF 208).

54. **Felcini M.** — The Search for Higgs Particles at LEP, hep-ex/9907049 (1999).

55. The ALEPH Collaboration, Search for Neutral Higgs Bosons in e^+e^- Collisions at $\sqrt{s} \leq 196$ GeV, hep-ex/9908016 (1999).

56. **Mcnamara P.** — Talk given at LEP EXPERIMENTS COMMITTEE; CERN, 7 September 1999.

57. **Gross E. et al.** — Prospects for the Higgs Boson Search in Electron-Positron Collisions at LEP 200, CERN-EP/98-094.

58. **Georgi H. et al.** — Phys. Rev. Lett., 1978, v.40, p.692.

59. **Djouadi A., Spira M., Zervas P.M.** — Phys. Lett., 1991, v.B264, p.440;
Spira M., Djouadi A., Graudenz D., Zervas P.M. — Nucl. Phys., 1995, v.B453, p.17.

60. **Cahn R.N., Dawson S.** — Phys. Lett., 1994, v.B136, p.196;
Hikasa K. — Phys. Lett., 1985, v.B164, p.341;
Altarelli G., Mele B., Pitolli F. — Nucl. Phys., 1987, v.B287, p.205;
Han T., Valensia G., Willenbrock S. — Phys. Rev. Lett., 1992, v.69, p.3274.

61. **Glashow S.L., Nanopoulos D.V., Yildiz A.** — Phys. Rev., 1978, v.D18, p.1724.

62. **Kunszt Z.** — Nucl. Phys., 1984, v.B247, p.339;
Gunion J.F. — Phys. Lett., 1991, v.B253, p.269;
Marciano W.J., Paige F.E. — Phys. Rev. Lett., 1991, v.66, p.2433.

63. **Quigg C.** — Physics Opportunities in Fermilab's Futures, FERMILAB-FN-676, March 1999.

64. **Montgometry H.E.** — Physics with the Main Injector, hep-ex/9904019.

65. **Tao Han, Turcot A.S., Ren-Jie Zhang** — Exploiting $h \to W^*W^*$ Decays at the Upgraded Fermilab Tevatron, FERMILAB, MADPH-08-1094 (1998), hep-ph/9812275 (1998).

66. The Large Hadron Collider, CERN/AC/95-05.

67. CMS, Technical Proposal, CERN/LHCC/94-38 LHCCP1, 15 December 1994.

68. ATLAS, Technical Proposal, CERN/LHCC/94-43 LHCCP2, 15 December 1994.

69. As a review of physics to be studied at LHC see, for example:
Krasnikov N.V., Matveev V.A. — Phys. Part. Nucl., 1997, v.28, p.441.

70. **Seez C.** — $H \to \gamma\gamma$; An Update, CMS TN/94-289 (1994).

71. **Lassila-Perrini K.** — The Reconstruction of Higgs $\to \gamma\gamma$ in CMS, CMS CR/97-006 (1997).

72. **Abdullin S., Starodumov A., Stepanov N.** — Study of the Associated Production Modes WH and $t\bar{t}H$ in CMS, CMS TN/93-86 (1993).

73. **Abdullin S. et al.** — Possibilities to Improve the Observability of SM Light Higgs in the $\gamma\gamma$ Channel, CMS TN/94-247 (1994).

74. **Iashvili I. et al.** — Study of the $H \to ZZ^* \to 4l^{\pm}$ Channel in CMS, CMS TN/95-059(1995).

75. **Charlot C., Nikitenko A., Puljak I., Soric I.** — Comparison of Fixed Window and Clusterization Algorithms for $Z \to e^+e^-$ and $H \to 4e^{\pm}$ in CMS $PbWO_4$ Crystal ECAL for Higgs Mass 170 and 130 GeV, CMS TN/95-101 (1995).

76. **Bomestar D. et al.** — Study of the $H \to ZZ \to 4l^{\pm}$ with Full GEANT Simulation of CMS Detector, CMS TN/94-018 (1994).

77. **Dzelalija M., Antonovic Z., Kinnunen R.** — Study of the Heavy $H \to ZZ \to 4l^{\pm}$ in CMS, CMS TN/95-076 (1995).

78. **Abdullin S., Stepanov N.** — Towards Self-Consistent Scenario of the Heavy Higgs Observability via the Channels $l\nu jj$ and $lljj$ at CMS, CMS TM/94-178 (1994).

79. **Kinnunen R., Denegri D.** — Expected SM/SUSY Higgs Observability in CMS, CMS Note 1997/057 (1997).

80. **Drollinger V., Muller T., Kinnunen R.** — Possibilities of $t\bar{t}H^0$ Event Reconstruction, CMS Note 1999/001 (1999).

81. **Spira M., Dittmar M.** — Standard Model Higgs Cross Sections (NLO) and PYTHIA, CMS Note 1997/080 (1997).

82. **Dubinin M.N., Ilyin V.A., Savrin V.I.** — Light Higgs Boson Signal at LHC in the Reactions $pp \to \gamma\gamma + \text{jet}$ and $pp \to \gamma\gamma + \text{lepton}$, CMS Note 1997/101;
Abdullin S. et al. — Phys. Lett., 1998, v.B431, p.410.

83. **Dittmar M., Dreiner H.** — Phys. Rev., 1997, v.D55, p.167 [hep-ph/9608317]; LHC Higgs Search with $l^+\nu l^-\bar{\nu}$ Final States, CMS Note 1997/083.

84. **Green D. et al.** — Search for the Standard Model Higgs Boson with $M_H \approx 170\ \text{GeV}/c^2$ in W^+W^- Decay Mode, CMS Note 1998/089.

85. **Iashvili I. et al.** — Study of the $H \to 4l^{\pm}$ Channel in CMS, CMS Note 1995/059.

86. **Stepanov N.** — Search for Heavy Higgs via the $H \to ll\nu\nu$ Channel, CMS TN/93-87 (1993);
Stepanov N., Starodumov A. — Search for Higgs in the TEV Region, CMS-TN/92-49 (1992).

87. **Zmushko S., Frodeavaux D., Poggioli L.** — $H \to WW \to l\nu jj$ and $H \to ZZ \to lljj$. Particle Level Studies, ATLAS Internal Note PHYS-No-103 (1997).

88. **Poggioli L.** — $H \to ZZ^* \to 4$ Leptons. A Comparison of ATLAS and CMS Potentials, ATLAS Internal Note, PHYS-No-066 (1995).

89. **Froidevaux D., Gianotti F., Richter-Was E.** — Comparison of the ATLAS and CMS Discovery Potential for the $H \to \gamma\gamma$ Channel at the LHC, ATLAS Internal Note PHYS-No-64 (1995).

90. **Cavasinni V., Costanzo D., Lami S., Spano F.** — Search for $H \to WW \to l\nu jj$ with the ATLAS Detector ($m_H = 300 - 600$ GeV), ATLAS Internal Note,ATL-PHYS-98-127 (1998).

91. **Linossier O., Poggioli L.** — $H^0 \to ZZ^* \to 4l$ Channel, in ATLAS. Signal Reconstruction and Reducible Backgrounds Rejection, ATLAS Note PHYS-No-101 (1997).

92. **Zmushko S.** — $H \to \gamma\gamma$ in Association with Jets, ATLAS Internal Note ATL-PHYS-99-009(1999).

93. **Richter-Was E., Sapinski M.** — Search for the SM and MSSM Higgs Boson in the $t\bar{t}H$, $HH \to b\bar{b}$ Channel, ATL-PHYS-98-132 (1998).

94. **Savard P., Azuelos G.** — The Discovery Potential of a Heavy Higgs ($M_H = 800$ GeV) Using Full GEANT Sumulations of ATLAS, ATL-PHYS-98-128 (1998).

95. **Linossier O., Zitoun R.** — $H_0 \to ZZ^* \to 4\ l$ Channel, in ATLAS - A Complementary Study of the ZZ^* Background, ATL-PHYS-96-096 (1996).

96. **Tisserand V.** — The Higgs to Two-Photon Decay in the ATLAS Detector UPDATED, ATL-PHYS-96-091.

97. **Bityukov S.I., Krasnikov N.V.** — Mod. Phys. Lett., 1998, v.A13, p.3235;
Bityukov S.I., Krasnikov N.V. — Observability and Probability of Discovery in Future Experiments, hep-ph/9908402 (1999), CMS IN Note 1999/027.

98. **Rainwater D., Zeppenfeld D.** — Observing $H \to W^{(*)}W^{(*)} \to e^{\pm}\mu^{\mp}p_T^{\text{mis}}$ in Weak Boson Fusion with Dual Forward Jet Tagging at the CERN LHC, hep-ph/9906218 (1999).

99. **Rainwater D., Hagiwara K., Zeppenfeld D.** — Searching for $H \to \tau\tau$ in Weak Boson Fusion, hep-ph/9808468 (1998).